The Astrophysical Journal, 769:49 (16pp), 2013 May 20 doi:10.1088/0004-637X/769/1/49

STARDUST INVESTIGATION INTO THE CR CHONDRITE GROVE MOUNTAIN 021710

Xuchao Zhao[1], Christine Floss[2], Yangting Lin[1,4], and Maitrayee Bose[3]
[1] Key Laboratory of the Earth's Deep Interior, Institute of Geology and Geophysics, Chinese Academy of Sciences, 19 Beituchengxi Road, Beijing 100029, China; linyt@mail.igcas.ac.cn
[2] Laboratory for Space Sciences and Physics Department, Washington University, One Brookings Drive, St. Louis, MO 63130, USA
[3] Department of Chemistry and Biochemistry, Arizona State University, P.O. Box 871604, Tempe, AZ 85287, USA
Received 2013 February 3; accepted 2013 April 5; published 2013 May 3

ABSTRACT

We report the presolar grain inventory of the CR chondrite Grove Mountain 021710. A total of 35 C-anomalous grains (∼236 ppm) and 112 O-anomalous grains (∼189 ppm) were identified in situ using NanoSIMS ion imaging. Of 35 C-anomalous grains, 28 were determined to be SiC grains by Auger spectroscopy. Seven of the SiC grains were subsequently measured for N and Si isotopes, allowing classification as one nova grain, one Y grain, one Z grain, and four mainstream grains. Eighty-nine out of 112 O-anomalous grains belong to Group 1, indicating origins in low-to-intermediate-mass red giant and asymptotic giant branch stars. Twenty-one are Group 4 grains and have origins in supernovae. Auger spectroscopic elemental measurements of 35 O-anomalous grains show that 33 of them are ferromagnesian silicates. They have higher Mg/(Mg+Fe) ratios than those reported in other meteorites, suggesting a lower degree of alteration in the nebula and/or asteroid parent bodies. Only two oxide grains were identified, with stoichiometric compositions of $MgAl_2O_4$ and SiO_2, respectively. The presolar silicate/oxide ratio of GRV 021710 is comparable with those of the CR3 chondrites (QUE 99177 and MET 00426) and primitive interplanetary dust particles. In order to search for presolar sulfides, the meteorite was also mapped for S isotopes. However, no presolar sulfides were found, suggesting a maximum abundance of 2 ppm. The scarcity of presolar sulfides may be due to their much faster sputtering rate by cosmic rays compared to silicates.

Key words: astrochemistry – circumstellar matter – novae, cataclysmic variables – nuclear reactions, nucleosynthesis, abundances – stars: winds, outflows – supernovae: general

Online-only material: color figures

1. INTRODUCTION

Primitive meteorites contain small circumstellar dust grains that condensed in the outflows of asymptotic giant branch (AGB) and red giant (RG) stars, as well as in supernovae ejecta. These grains, which survived homogenization in the solar nebula, can be extracted from the parent meteorites and studied in detail using multiple methods. To date, various presolar phases including nanodiamonds, silicon carbide, graphite, silicon nitride, silicates, and oxides have been identified in different groups of meteorites, as well as interplanetary dust particles (IDPs) and micrometeorites (e.g., Zinner 2007). Isotopic studies of these presolar grains, combined with elemental analyses, can provide detailed information not only about the stellar nucleosynthetic processes of their parent sources, but also about the chemical and physical conditions of stellar atmospheres during condensation, as well as secondary processes that they underwent subsequent to their formation.

The CR group is generally considered to be one of the most primitive meteorite classes (Krot et al. 2002). Although most meteorites in this group have undergone extensive aqueous alteration, presolar grain investigations of some CR3 chondrites show the highest abundances among all primitive meteorites that have been investigated for presolar phases (e.g., Floss & Stadermann 2009a, 2009b; Nguyen et al. 2010). The first studies of the CR2 chondrites (Renazzo and NWA 530) indicated low abundances of presolar grains (Nagashima et al. 2004; Floss & Stadermann 2005); however, a recent study by Leitner et al. (2012) revealed much higher presolar grain concentrations in the CR2 chondrite NWA 852. Although NWA 852 has a very high abundance of presolar SiC grains, the abundance of its presolar O-anomalous grains is still lower than that of the CR3 chondrites. This may be due to the aqueous alteration that NWA 852 has experienced (Leitner et al. 2012). GRV 021710 was collected from Grove Mountain, East Antarctica, and is classified as a CR2 chondrite (Miao et al. 2007). With a complete fusion crust, it shows little terrestrial weathering. Although presolar silicates appear to be easily destroyed by secondary processes, the presence of abundant presolar grains in NWA 852 (Leitner et al. 2012) suggests that investigation of other CR2 chondrites is warranted. Detailed isotopic and elemental studies of presolar grains can help us to better understand the role that secondary processes played in altering or destroying them in CR chondrites. Moreover, it is interesting to note that the matrix in GRV 021710 contains abundant submicron-sized sulfide grains, similar to the sizes of the presolar silicates. Sulfide grains have been observed in the interstellar medium (ISM) and circumstellar shells around the low-to-intermediate mass stars (Tielens 2005; Kahane et al. 1988), but presolar sulfides have not yet been found in meteorites. Here, we report on the isotopic and chemical compositions of C- and O-anomalous grains identified in the CR chondrite GRV 021710 using combined NanoSIMS and Auger Nanoprobe analyses, as well as the results of S isotope imaging measurements. Preliminary results were reported in Zhao et al. (2011b).

2. EXPERIMENTAL

A polished thin section of the CR chondrite GRV 021710 was first surveyed with an optical microscope to select fine-grained matrix areas suitable for presolar grain searches.

[4] Author to whom any correspondence should be addressed.

Then, the Cameca NanoSIMS 50 at Washington University (WashU) was used to locate isotopic anomalies. A relatively high beam current (~100 pA) was initially used to presputter $12 \times 12\,\mu m^2$ matrix areas to remove the carbon coating. The measurements were done in raster imaging mode by scanning a focused Cs^+ primary ion beam (~1 pA, ~100 nm diameter) over $10 \times 10\,\mu m^2$ (256^2 pixels) matrix areas within the $12 \times 12\,\mu m^2$ presputtered regions. Negative secondary ions of both C and O isotopes ($^{12}C^-$, $^{13}C^-$, $^{16}O^-$, $^{17}O^-$, $^{18}O^-$) were collected simultaneously, along with secondary electrons (SE). Each measurement contained multiple (5−10) frames, with analysis times of ~20 minutes for each frame. The individual frames were added together to obtain a single image measurement after correction of possible position shift. All measurements were obtained in chained analysis mode, with automated stage movement to subsequent measurement areas. The total area of matrix analyzed was 10,700 μm^2. Carbon and oxygen isotopic compositions were normalized internally by assuming the average composition of surrounding matrix area to be solar. Grains were defined as presolar if their isotopic compositions differed from the solar values by more than 5σ and the isotopic anomaly was present in at least three consecutive image frames. In one case (following the identification of ^{13}C-rich grain M1R-6C), a second ($6 \times 6\,\mu m^2$; 256^2 pixels) measurement was done to define the isotopic composition of this grain more precisely. Corrections for the QSA (quasi-simultaneous arrival) effect show no significant effects on the O isotopic ratios, within the given errors. The measurement procedures and data processing methods are discussed in detail by Stadermann et al. (2005). Following Auger elemental measurements (see below), we also carried out S isotopic analyses in raster imaging mode with the Cameca NanoSIMS 50L at the Institute of Geology and Geophysics, Chinese Academy of Sciences (IGGCAS). The measurement conditions and analysis procedures were similar to the C–O isotopic mapping performed on the WashU NanoSIMS 50. The S isotopic compositions were corrected for the QSA effect ($K = 0.08$), which was on the order of ~40‰. The three O isotopes (in a few cases, only ^{16}O and ^{18}O) and ^{12}C were measured along with ^{32}S, ^{33}S, and ^{34}S. The total area of matrix mapped for O–S isotopes was 36,200 μm^2.

Subsequent to the NanoSIMS ion imaging measurements, presolar grains identified in the WashU NanoSIMS were measured using the PHI 700 Auger Nanoprobe at Washington University to characterize their chemical compositions. Before the Auger measurement, a defocused Ar^+ ion beam (2 kV, 1 μA) was used to remove possible contamination on the sample surface. Since high beam current can cause sample damage on the grain surface and possible artifacts in the Auger spectra (Stadermann et al. 2009), we used a low beam current (10 kV, 0.25 nA) to carry out the Auger elemental analyses in the energy range 50–1750 eV. Multiple scans of each grain were added to obtain a single average Auger spectrum. Seven-point smoothing and a Savitsky–Golay differentiation routine was then used to differentiate the averaged spectrum before peak identification and quantification. For C-anomalous grains, the Auger spectra were only used to qualitatively identify the mineral type of presolar grains. Quantitative compositions of the O-anomalous grains were calculated on the basis of the peak-to-peak heights in the Auger spectra and normalized using elemental sensitivity factors. The sensitivity factors for O (0.194), Si (0.121), Mg (0.234), Fe (0.150), Ca (0.626), and Al (0.160) were carried out from repeated Auger elemental measurements on a series of powdered silicate standards (Stadermann et al. 2009). The sensitivity factors have 1σ uncertainties of: O, 3.6%; Si, 11.0%; Fe, 11.2%; Mg, 9.4%; Al, 24.9%; and Ca, 10.8% (Stadermann et al. 2009). Since all sensitivity factors listed above were obtained from silicate standards, the compositions of oxide grains may have higher uncertainties (Stadermann et al. 2009). Additional errors from the presence of sample charging, background noise, and surface contaminants are not included. High-resolution (10–20 nm) elemental distribution maps ($2 \times 2\,\mu m^2$, $3 \times 3\,\mu m^2$, or $5 \times 5\,\mu m^2$; 256^2 pixels) were also obtained for selected major elements (e.g., C, N, O, Mg, Al, Si, S, Ca, Fe) for most grains. Auger elemental mapping was obtained by scanning a 10 kV 5 nA primary beam over the areas of interest, and generally consisted of 5−30 scans, depending on the sensitivity of the element being mapped. These maps can provide detailed information about the elemental distributions within and around the presolar grains.

Finally, selected SiC grains were measured for C, N, and Si isotopes using the Cameca NanoSIMS 50L at IGGCAS. A 16 keV Cs^+ primary ion beam of ~1.3 pA intensity was used, and the negative secondary ions of ^{12}C, ^{13}C, $^{12}C^{14}N$, $^{12}C^{15}N$, ^{28}Si, ^{29}Si, and ^{30}Si were collected simultaneously. All measurements were done in grain mode, in which $10 \times 10\,\mu m^2$ measurement areas were initially located and imaged in $^{12}C^-$, $^{13}C^-$, and $^{28}Si^-$. For these measurements, synthetic SiC and Si_3N_4 grains (0.5−1.0 μm) were used as isotopic standards for tuning and normalization of the isotopic ratios.

3. RESULTS

3.1. NanoSIMS Ion Mapping

From the NanoSIMS isotopic mapping, we identified 35 and 112 grains with C and O isotopic anomalies, respectively. All 35 C-anomalous grains and 35 of the 112 O-anomalous grains were identified within 10,700 μm^2 from the C–O isotopic mapping performed on the WashU NanoSIMS 50, whereas the remaining 77 O-anomalous grains were found within 36,200 μm^2 from the O–S isotopic mapping with the IGGCAS NanoSIMS 50L.

Table 1 lists the isotopic data for the 35 C-anomalous grains. Twenty-eight grains have $^{12}C/^{13}C$ ratios ranging from 29 to 76, similar to mainstream SiC grains. Six grains are ^{13}C-depleted, with $^{12}C/^{13}C$ ratios between 103 and 124. The remaining grain, M1R-6c, is highly ^{13}C-enriched ($^{12}C/^{13}C = 4.18 \pm 0.03$), within the range of type A+B or nova SiC grains (Table 1).

Table 2 lists the information for the 112 O-anomalous grains, including isotopic compositions and sizes. The O isotopic compositions of the 112 O-anomalous grains are also plotted in Figure 1. Eighty-six of them can be classified as Group 1 according to the definition of Nittler et al. (1997), with $^{17}O/^{16}O$ ratios ranging from 4.20×10^{-4} to 2.34×10^{-3} and solar to slightly subsolar $^{18}O/^{16}O$ ratios ($1.27-2.29 \times 10^{-3}$). A few grains in this group have $^{18}O/^{16}O$ ratios close to 1×10^{-3}, indicating that they probably belong to the Group 2 category (see Section 4.1). Two grains are indeed Group 2 grains, with $^{18}O/^{16}O$ ratios less than 1×10^{-3} ($7.53-9.33 \times 10^{-4}$). Nineteen grains are ^{18}O-rich ($^{18}O/^{16}O = 2.20-4.59 \times 10^{-3}$) and belong to Group 4. One grain (M6C-18) of this group shows slight depletion in ^{17}O, but we still classify it into Group 4 on the basis of its $^{18}O/^{16}O$ ratio of 2.31×10^{-3}. The remaining five grains, in which only $^{18}O/^{16}O$ ratios have been determined, include two Group 4 and three Group 1 grains (Table 2, flagged with question marks).

Table 1
C-anomalous Grains from GRV 021710

Grain	Size[a] (nm)	$^{12}C/^{13}C$	$\delta^{13}C/^{12}C$(‰)[b]	Types[c]
		SiC		
M1A2–6c	1060 × 800	43.8 ± 0.2	1034 ± 4	MS
M1E2–3c	170 × 120	45.3 ± 2.0	964 ± 43	*MS, Z*
M1F-6c	650 × 400	57.3 ± 0.4	554 ± 4	Z
M1G-6c	150 × 120	54.5 ± 1.3	633 ± 15	*MS, Z*
M1M-2 c-a	190 × 120	67.7 ± 2.8	314 ± 13	*MS, Z*
M1M-2 c-b	270 × 160	70.2 ± 2.7	269 ± 10	*MS, Z*
M1M-2 c-c	220 × 120	70.2 ± 2.7	269 ± 10	*MS, Z*
M1Nc-a	210 × 150	29.3 ± 0.5	2033 ± 31	*MS, Z*
M1Nc-b	150 × 130	124 ± 5	−283 ± 11	*Y, X*
M1P-2 c-a	290 × 160	63.0 ± 1.4	412 ± 9	*MS, Z*
M1Q-3c	400 × 260	68.7 ± 1.8	295 ± 8	*MS, Z*
M1R-6c	460 × 390	4.18 ± 0.03	20, 301 ± 142	Nova
M1S-2c	210 × 120	57.0 ± 2.8	561 ± 27	*MS, Z*
M1T-3c	260 × 260	25.3 ± 0.6	2518 ± 64	MS
M1U-6c	380 × 320	61.9 ± 1.4	438 ± 10	*MS, Z*
M4B-3c	390 × 310	112 ± 1	−208 ± 2	Y
M3J-4c	470 × 470	43.9 ± 0.4	1028 ± 8	MS
M3L-9c	390 × 230	60.3 ± 0.6	475 ± 5	MS
M1E2–6c	160 × 110	60.9 ± 2.5	460 ± 19	*MS, Z*
M1P-1c	140 × 140	49.4 ± 2.9	802 ± 48	*MS, Z*
M1Q-2c	140 × 140	54.2 ± 2.4	643 ± 29	*MS, Z*
M1R-1c	150 × 140	51.3 ± 2.8	734 ± 41	*MS, Z*
M1S-4c	150 × 120	65.6 ± 4.2	356 ± 23	*MS, Z*
M1T-2c	130 × 110	31.7 ± 1.3	1807 ± 76	*MS, Z*
M1M-4c	230 × 160	33.4 ± 0.5	1661 ± 24	*MS, Z*
M1N2c	170 × 160	67.4 ± 2.3	321 ± 11	*MS, Z*
M1S-5c	140 × 110	56.1 ± 3.2	588 ± 34	*MS, Z*
M1T-5c	170 × 140	50.8 ± 2.7	752 ± 39	*MS, Z*
		Carbonaceous		
M1B-4c	390 × 350	113 ± 3	−214 ± 6	
M1B2–3c	200 × 140	103 ± 2	−133 ± 3	
M1F-3c	260 × 240	65.2 ± 2.9	365 ± 16	
M1G-3c	380 × 230	109 ± 3	−186 ± 5	
M1P-2 c-b	360 × 340	76.1 ± 1.8	169 ± 4	
M1Q-7c	290 × 160	112 ± 4	−205 ± 7	
		Sputtered away?		
M1E2–1c	*550 × 470*	107 ± 2	− 164 ± 3	

Notes. Errors are 1σ.
[a] Grain sizes in italics are determined by NanoSIMS ion images.
[b] Deviation from normal in parts per thousand: $(R_{meas}/R_{std} - 1) \times 1000$ (‰).
[c] MS: mainstream; grains in italics are those for which the identification is less certain (see the text for details).

Table 2
O-anomalous Grains from GRV 021710

Grain	Size[a] (nm)	$^{17}O/^{16}O$[b] (10^{-4})	$^{18}O/^{16}O$ (10^{-3})	Group
M1A3–3	280 × 240	5.70 ± 0.18	2.04 ± 0.01	1
M1A3–4	200 × 140	5.70 ± 0.18	2.04 ± 0.01	1
M1B-2	380 × 300	5.25 ± 0.20	1.86 ± 0.01	1
M1B-4	240 × 150	4.80 ± 0.18	1.97 ± 0.01	1
M1B2–2	300 × 190	5.67 ± 0.25	1.83 ± 0.01	1
M1B2–4	350 × 210	6.08 ± 0.20	1.43 ± 0.01	1
M1B2–5a	160 × 120	6.73 ± 0.21	2.04 ± 0.01	1
M1B2–5b	250 × 190	7.34 ± 0.32	1.31 ± 0.02	1
M1D-1	230 × 180	3.90 ± 0.16	2.28 ± 0.06	4
M1D-2	300 × 260	4.26 ± 0.20	2.73 ± 0.08	4
M1E2–3	140 × 120	5.74 ± 0.15	1.74 ± 0.08	1
M1E2–5	180 × 140	4.02 ± 0.18	2.56 ± 0.07	4
M1K-4	430 × 300	5.80 ± 0.17	1.52 ± 0.01	1
M1M-2	300 × 180	3.80 ± 0.14	2.30 ± 0.01	4
M1M-3	400 × 270	9.62 ± 0.26	1.57 ± 0.02	1
M1N3	210 × 160	12.64 ± 0.38	2.08 ± 0.03	1
M1N6–1	430 × 360	6.03 ± 0.14	1.85 ± 0.01	1
M1P-1	250 × 190	5.01 ± 0.25	2.05 ± 0.01	1
M1P-5	310 × 250	7.51 ± 0.26	4.59 ± 0.01	4
M1P-6	210 × 190	10.77 ± 0.38	4.20 ± 0.02	4
M1Q-7	520 × 330	8.63 ± 0.24	0.93 ± 0.02	2
M1Q-8	270 × 270	5.71 ± 0.20	1.98 ± 0.01	1
M1R-1a	170 × 150	5.84 ± 0.24	1.97 ± 0.01	1
M1R-1b	180 × 140	4.95 ± 0.23	1.65 ± 0.01	1
M1R-1d	200 × 140	4.33 ± 0.17	2.28 ± 0.01	4
M1R-7	260 × 220	5.02 ± 0.29	1.44 ± 0.02	1
M1S-2	220 × 170	6.24 ± 0.24	1.43 ± 0.02	1
M1S-4	330 × 210	5.52 ± 0.22	1.80 ± 0.01	1
M1T-6	470 × 390	6.25 ± 0.37	1.94 ± 0.02	1
M1U-1	180 × 150	5.29 ± 0.27	3.12 ± 0.01	4
M1U-2a	260 × 160	6.73 ± 0.39	2.11 ± 0.02	1
M1U-2b	390 × 320	4.26 ± 0.26	2.74 ± 0.01	4
M1U-3	460 × 270	5.84 ± 0.26	1.81 ± 0.01	1
M1U-6	330 × 210	8.30 ± 0.38	1.98 ± 0.02	1
M1U-7	320 × 200	6.13 ± 0.30	2.03 ± 0.01	1
M1W-1	*310 × 310*	11.27 ± 0.55	2.00 ± 0.07	1
M2A-1	*420 × 380*	4.41 ± 0.13	1.60 ± 0.03	1
M2C-2a	*340 × 340*	4.89 ± 0.14	1.98 ± 0.03	1
M2C-2b	*270 × 250*	4.73 ± 0.17	2.00 ± 0.04	1
M2D-1	*390 × 390*	6.75 ± 0.13	1.86 ± 0.06	1
M2D-2	*460 × 410*	6.06 ± 0.26	1.91 ± 0.02	1
M2D-6	*340 × 340*	5.89 ± 0.13	2.16 ± 0.03	1
M2D-13	*570 × 520*	5.99 ± 0.11	1.40 ± 0.02	1
M2D-17	*300 × 300*	4.79 ± 0.15	2.69 ± 0.05	4
M2D-20	*410 × 360*	4.92 ± 0.15	2.08 ± 0.04	1
M2G-3	*430 × 380*	5.41 ± 0.16	2.09 ± 0.03	1
M2G-10a	*500 × 450*	4.14 ± 0.14	2.37 ± 0.03	4
M2G-10b	*300 × 290*	3.80 ± 0.23	1.76 ± 0.05	1
M2H-10	*230 × 200*	5.71 ± 0.34	1.98 ± 0.06	1
M2K-9	*350 × 350*	5.22 ± 0.22	1.93 ± 0.04	1
M2L-5	*390 × 390*	9.99 ± 0.48	1.95 ± 0.05	1
M2L-C-1	*350 × 350*	8.37 ± 0.60	1.94 ± 0.04	1
M2M-1	*300 × 260*	10.92 ± 0.59	2.02 ± 0.04	1
M2M-2	*330 × 280*	5.76 ± 0.27	1.97 ± 0.05	1
M2M-4	*420 × 390*	6.48 ± 0.23	1.57 ± 0.03	1
M2M-7	*350 × 350*	5.95 ± 0.23	1.56 ± 0.04	1
M2M-8	*220 × 220*	6.63 ± 0.45	1.38 ± 0.06	1
M2M-16	*380 × 350*	7.56 ± 0.30	2.00 ± 0.05	1
M2N-4	*420 × 420*	6.18 ± 0.24	2.01 ± 0.04	1
M3C-3	*390 × 390*	6.51 ± 0.28	1.95 ± 0.05	1
M3C-4	*310 × 310*	5.94 ± 0.33	1.98 ± 0.07	1
M3C-7a	*420 × 420*	5.40 ± 0.75	1.95 ± 0.06	1
M3C-7b	*380 × 350*	6.00 ± 0.27	2.07 ± 0.04	1
M3E-1	*300 × 270*	7.28 ± 0.34	2.14 ± 0.05	1
M3E-4	*380 × 350*	4.99 ± 0.20	1.66 ± 0.03	1

Sulfur-32, 33, 34 mapping of the sample shows abundant submicron-sized (∼300 nm) sulfide grains, similar in size to the O-anomalous grains. Sulfur isotopic ratios of the S-rich grains vary between 15‰−50‰ for $\delta^{34}S$ and 10‰−30‰ for $\delta^{33}S$; however, there are no significant S isotopic anomalies identified in any of the areas measured (total area = 36,200 μm^2). We can calculate an upper limit of ∼2 ppm for the abundance of presolar sulfides in this meteorite.

Presolar grain abundances of GRV 021710 were calculated based on the total area of presolar grains and the total matrix area analyzed. The areas of the presolar grains were calculated on the basis of either the Auger SE images or the NanoSIMS images if an Auger SE image was not available. The 35 C-anomalous grains found within 10,700 μm^2 result in a matrix-normalized abundance of 236 ± 40 ppm (error is based on counting

Table 2
(Continued)

Grain	Size[a] (nm)	$^{17}O/^{16}O^{b}$ (10^{-4})	$^{18}O/^{16}O$ (10^{-3})	Group
M3F-3	*380 × 380*	23.42 ± 1.82	1.95 ± 0.06	1
M5A-3	*470 × 240*	n.m.	1.41 ± 0.02	1 (?)
M5A-13	*390 × 320*	n.m.	1.57 ± 0.04	1 (?)
M5A-14a	*200 × 190*	n.m.	2.27 ± 0.07	4 (?)
M5A-14b	*250 × 220*	n.m.	1.73 ± 0.07	1 (?)
M5A-15	*320 × 240*	n.m.	2.38 ± 0.09	4 (?)
M5B-5	*220 × 220*	6.35 ± 0.30	2.06 ± 0.05	1
M5B-10	*220 × 220*	3.88 ± 0.22	2.26 ± 0.05	4
M5B-11	*390 × 390*	6.62 ± 0.21	2.03 ± 0.01	1
M5B-16	*320 × 320*	4.13 ± 0.32	2.21 ± 0.04	4
M5C-9	*590 × 390*	5.77 ± 0.36	3.46 ± 0.10	4
M5C-12	*720 × 720*	4.08 ± 0.05	2.20 ± 0.01	4
M5D-4	*220 × 220*	5.80 ± 0.29	1.54 ± 0.05	1
M5D-7	*250 × 220*	4.83 ± 0.23	1.78 ± 0.04	1
M5D-10	*320 × 290*	4.19 ± 0.15	2.12 ± 0.03	4
M5E-2	*280 × 250*	6.65 ± 0.25	1.99 ± 0.04	1
M5E-3	*190 × 190*	7.27 ± 0.35	1.95 ± 0.05	1
M5E-5	*310 × 310*	4.71 ± 0.18	1.99 ± 0.03	1
M5E-6	*220 × 220*	5.43 ± 0.27	1.66 ± 0.05	1
M5E-12	*310 × 310*	5.55 ± 0.19	1.99 ± 0.03	1
M5E-17	*360 × 360*	5.11 ± 0.16	1.68 ± 0.03	1
M6A-1a	*390 × 320*	15.24 ± 0.59	1.97 ± 0.02	1
M6A-1b	*240 × 160*	4.89 ± 0.20	1.97 ± 0.07	1
M6A-1c	*240 × 160*	3.71 ± 0.37	2.50 ± 0.05	4
M6B-1	*390 × 390*	6.90 ± 0.35	2.04 ± 0.02	1
M6B-6	*470 × 240*	5.50 ± 0.13	1.41 ± 0.04	1
M6B-9	*390 × 390*	9.04 ± 0.81	0.75 ± 0.02	2
M6C-4	*790 × 470*	14.10 ± 0.21	2.29 ± 0.03	1
M6C-5a	*240 × 240*	7.21 ± 0.78	1.88 ± 0.03	1
M6C-5b	*200 × 200*	5.95 ± 0.91	2.06 ± 0.03	1
M6C-5c	*200 × 200*	5.29 ± 0.29	1.84 ± 0.07	1
M6C-8	*470 × 390*	7.31 ± 0.58	1.27 ± 0.04	1
M6C-18	*320 × 240*	3.48 ± 0.10	2.31 ± 0.03	4
M6C-19	*390 × 240*	7.02 ± 0.35	1.98 ± 0.07	1
M6D-1	*470 × 470*	20.74 ± 0.50	1.94 ± 0.05	1
M6F-1	*240 × 240*	5.14 ± 0.13	1.94 ± 0.03	1
M6F-3a	*240 × 240*	8.27 ± 1.09	1.99 ± 0.04	1
M6F-3b	*240 × 240*	8.04 ± 0.73	1.97 ± 0.02	1
M6F-4	*320 × 320*	4.26 ± 0.12	2.25 ± 0.05	4
M6F-10	*240 × 240*	5.10 ± 0.17	2.05 ± 0.01	1
M6F-11	*240 × 240*	5.88 ± 0.14	1.67 ± 0.02	1
M6F-22	*320 × 320*	4.91 ± 0.11	1.98 ± 0.03	1
M6F-25	*240 × 240*	4.20 ± 0.21	1.75 ± 0.03	1
M6F-28	*240 × 240*	4.84 ± 0.13	1.99 ± 0.04	1
M6G-2a	*470 × 470*	8.90 ± 1.89	2.00 ± 0.04	1
M6G-2b	*320 × 320*	5.58 ± 0.27	1.60 ± 0.05	1
M6G-2c	*240 × 240*	4.87 ± 0.30	2.06 ± 0.03	1

Notes.
[a] Grain sizes in italics are determined by NanoSIMS ion images.
[b] "n.m.": not measured. Errors are 1σ.

statistics only). The total matrix area mapped for O isotopes was 46,900 μm^2, resulting in an abundance of 189 ± 18 ppm for the 112 O-anomalous grains. Based on the Auger elemental results (discussed below), we can also obtain abundances for different presolar phases: 182 ± 34 ppm for SiC, 35 ± 14 ppm for carbonaceous grains, and 165 ± 29 and 9 ± 6 ppm for presolar silicates and oxides, respectively.

3.2. Elemental Analysis

Thirty-five O-anomalous grains and 35 C-anomalous grains identified with the WashU NanoSIMS were measured for their elemental compositions with the Auger Nanoprobe. Based on the Auger elemental results, we identified 33 ferromagnesian silicates, 1 oxide, 1 SiO_2, 28 SiC, and 6 carbonaceous grains. One C-anomalous grain could not be located in the Auger Nanoprobe and was probably sputtered away during the NanoSIMS measurement.

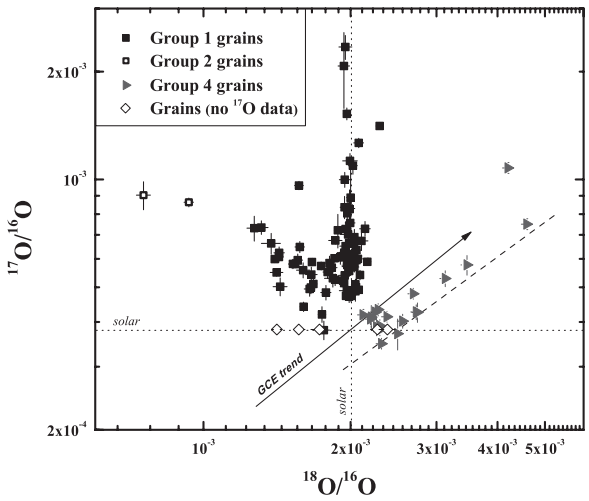

Figure 1. Oxygen three-isotope plot showing O-anomalous grains from GRV 021710. The dotted lines indicate solar values. The solid line labeled "GCE" indicates the expected galactic chemical evolution of oxygen isotopic ratios with increasing metallicity (Timmes et al. 1995). The dashed line near the "GCE" line is taken from Nittler (2007) and shows mixing between the ^{16}O-rich interior zones of a 15 $M_\odot$ supernova and the He/C zone and H envelope. Errors are 1σ (Table 2).

3.2.1. Presolar SiC/Carbonaceous Grains

Figure 2 shows the SE image of SiC grain M1A2–6c and carbonaceous grain M1F-3c, along with Auger spectra and elemental distribution maps used to characterize the grains.

The largest of the 28 SiC grains we found is 1060 × 800 nm in size (Grain M1A2–6c, in Table 1). The Auger spectrum of this grain (Figure 2(a)) shows that O is present in addition to Si and C. In fact, O peaks are present in the spectra of all SiC grains identified in this study, probably due to the presence of a thin oxide layer that typically forms on the grains upon exposure to atmosphere. SiC grains can also be recognized easily from the Auger elemental distribution maps. As shown in Figure 2(a), the SiC grain exhibits relatively high concentrations of C and Si, but a low concentration of O. Most of our SiC grains are 120–460 nm in size (Table 1), except grain M1A2–6c (1060 × 800 nm) and grain M1F-6c (650 × 400 nm). The size distribution of our SiC grains is consistent with previous studies, indicating that most presolar SiC grains have sizes less than 500 nm (Zinner 2007).

Carbonaceous grains found in this study appear as irregular, dark material in SE images and have grain sizes (140−390 nm) similar to most SiC grains identified (Table 1). All these grains have compositions dominated by C, as shown by the Auger spectrum of grain M1F-3c in Figure 2(b). Oxygen is often also present in the Auger spectra of these grains, but it is hard to tell whether this O is intrinsic to the grains or reflects residual surface contamination.

3.2.2. Presolar Silicate/Oxide Grains

All of the silicate grains have Fe- and/or Mg-bearing compositions. Three grains also contain Ca. Table 3 lists the major element compositions, (Fe+Mg+Ca)/Si ratios, cation/O ratios, O/Si ratios, mg# ((Mg/Mg+Fe) × 100), and possible phase

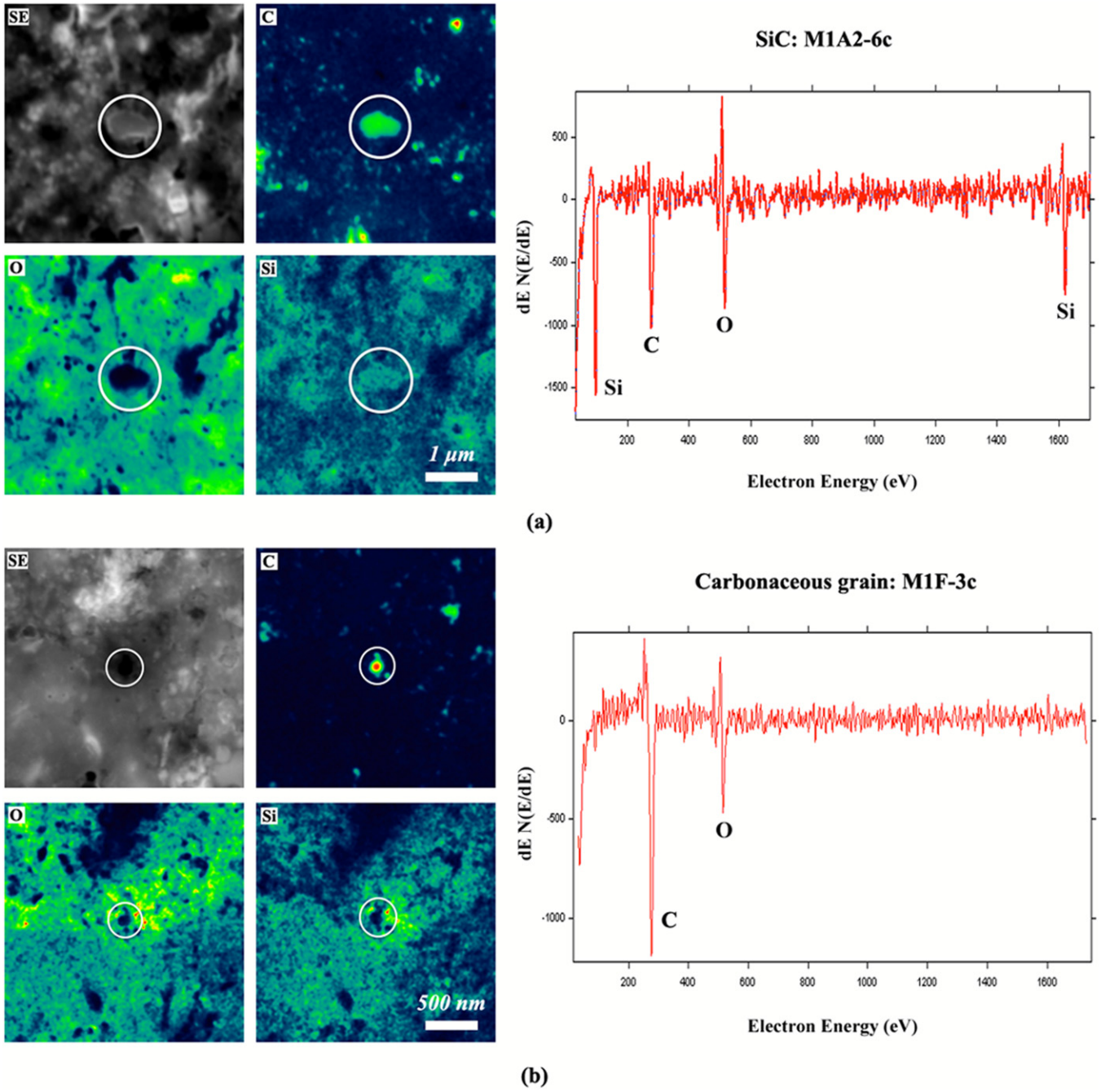

Figure 2. Secondary electron images, Auger spectra, and elemental maps of mainstream SiC grain M1A2–6c (a) and C-anomalous carbonaceous grain M1F-3c (b). Grains are circled in white.

(A color version of this figure is available in the online journal.)

identifications for these grains. Figure 3 shows (Fe+Mg+Ca)/Si ratios of the 33 presolar silicate grains. Olivine-like and pyroxene-like silicate grains were distinguished on the basis of (Fe+Mg+Ca)/Si ratios of 2 and 1 for olivine $(Mg, Fe)_2SiO_4$ and pyroxene $(Mg, Fe)SiO_3$, respectively. Ten grains have (Fe+Mg+Ca)/Si ratios that are consistent with olivine, and seven grains have (Fe+Mg+Ca)/Si ratios consistent with pyroxene (Table 3 and Figure 3). These classifications are also confirmed by the cation/O and O/Si ratios (olivine: 0.75 and 4, pyroxene: 0.67 and 3, respectively). The classifications of three grains (flagged with question marks in Table 3) identified as olivine are less certain because of significant deviation from the stoichiometric ratios. Grain M1A3–4 has higher cation/O (0.91) and lower O/Si (3.15) than olivine, whereas grains M1P-5 and M1Q-7 have lower cation/O (0.51−0.54) and higher O/Si (5.42−5.74). Figure 4 shows the SE images and Auger spectra of pyroxene-like grain M1B2–2 and olivine-like grain M1P-5. Pyroxene-like grain M1B2–2 is 300 × 190 nm in size and contains a minor amount of Ca (3.7 ± 0.4 at%). Olivine-like grain M1P-5 belongs to Group 4 and has the highest $^{18}O/^{16}O$ ratio observed in this study. This grain is 310 × 250 nm in size and contains no Fe. Like grain M1B2–2, pyroxene-like grain M1T-6 also contains a small amount of Ca (6.0 ± 0.6 at%). All olivine-like grains are Mg-rich, with mg#s ranging from 61 to

Table 3
Major Element Concentrations (at.%) and Phases of Presolar O-anomalous Grain from GRV 021710

Grain	O	Si	Mg	Fe	Ca	Al	(Fe+Mg±Ca)/Si	Cation/O	O/Si	mg#	Phase
M1A3–4	52.3 ± 1.9	16.6 ± 1.8	22.9 ± 2.2	8.2 ± 0.9			1.9 ± 0.2	0.91 ± 0.07	3.15	74	Olivine-like (?)
M1B-4	56.6 ± 2.0	15.5 ± 1.7	19.1 ± 1.8	8.8 ± 1.0			1.8 ± 0.2	0.77 ± 0.05	3.65	68	Olivine-like
M1M-2	56.5 ± 2.0	14.9 ± 1.6	21.2 ± 2.0	7.5 ± 0.8			1.9 ± 0.3	0.77 ± 0.06	3.79	74	Olivine-like
M1N6–1	57.5 ± 2.1	13.4 ± 1.5	20.0 ± 0.9	9.1 ± 1.0			2.2 ± 0.3	0.74 ± 0.05	4.29	69	Olivine-like
M1P-1	60.9 ± 2.2	13.0 ± 1.4	15.8 ± 1.5	10.2 ± 1.1			2.0 ± 0.3	0.64 ± 0.05	4.68	61	Olivine-like
M1P-5	65.0 ± 2.3	12.0 ± 1.3	23.0 ± 2.2				1.9 ± 0.3	0.54 ± 0.04	5.42	100	Olivine-like (?)
M1Q-7	66.1 ± 2.4	11.5 ± 1.3	22.4 ± 2.1				1.9 ± 0.3	0.51 ± 0.04	5.74	100	Olivine-like (?)
M1S-2	57.1 ± 2.1	13.3 ± 1.5	25.1 ± 2.4	4.5 ± 0.5			2.2 ± 0.3	0.75 ± 0.06	4.29	85	Olivine-like
M1S-4	61.4 ± 2.2	13.3 ± 1.5	25.3 ± 2.4				1.9 ± 0.3	0.63 ± 0.05	4.62	100	Olivine-like
M1U-7	57.4 ± 2.1	15.4 ± 1.7	20.4 ± 1.9	6.9 ± 0.8			1.8 ± 0.2	0.74 ± 0.05	3.72	75	Olivine-like
M1B2–2	55.0 ± 2.0	20.4 ± 2.2	11.0 ± 1.0	10.0 ± 1.1	3.7 ± 0.4		1.2 ± 0.2	0.82 ± 0.06	2.70	52	Pyroxene-like
M1E2–3	58.3 ± 2.1	20.5 ± 2.3	6.7 ± 0.6	14.5 ± 1.6			1.0 ± 0.1	0.72 ± 0.06	2.84	32	Pyroxene-like
M1E2–5	58.8 ± 2.1	22.0 ± 2.4	5.2 ± 0.5	14.0 ± 1.6			0.9 ± 0.1	0.70 ± 0.06	2.67	27	Pyroxene-like
M1N3	63.8 ± 2.3	18.4 ± 2.0	9.3 ± 0.9	8.5 ± 1.0			1.0 ± 0.1	0.57 ± 0.04	3.47	52	Pyroxene-like
M1T-6	59.0 ± 2.1	19.6 ± 2.2	7.1 ± 0.7	8.3 ± 0.9	6.0 ± 0.6		1.1 ± 0.1	0.69 ± 0.05	3.01	46	Pyroxene-like
M1U-2a	61.6 ± 2.2	17.8 ± 2.0	6.0 ± 0.6	14.6 ± 1.6			1.2 ± 0.2	0.62 ± 0.05	2.46	39	Pyroxene-like
M1U-6	59.8 ± 2.2	19.9 ± 2.2	10.2 ± 1.0	10.1 ± 1.1			1.0 ± 0.1	0.67 ± 0.05	3.01	50	Pyroxene-like
M1B-2	56.6 ± 2.0	16.8 ± 1.8	16.0 ± 1.5	10.6 ± 1.2			1.6 ± 0.2	0.77 ± 0.05	3.36	60	Intermediate
M1B2–4	61.7 ± 2.2	14.5 ± 1.6	16.5 ± 1.6	7.3 ± 0.8			1.6 ± 0.2	0.62 ± 0.04	4.26	69	Intermediate
M1B2–5a	57.7 ± 2.1	16.9 ± 1.9	16.5 ± 1.6	8.8 ± 1.0			1.5 ± 0.2	0.73 ± 0.05	3.41	65	Intermediate
M1B2–5b	56.8 ± 2.0	18.5 ± 2.0	15.3 ± 1.4	9.5 ± 1.1			1.3 ± 0.2	0.76 ± 0.06	3.07	62	Intermediate
M1D-1	58.7 ± 2.1	16.7 ± 1.8	17.0 ± 1.6	7.7 ± 0.9			1.5 ± 0.2	0.71 ± 0.05	3.51	69	Intermediate
M1U-1	60.9 ± 2.2	16.7 ± 1.8	10.9 ± 1.0	11.6 ± 1.3			1.3 ± 0.2	0.64 ± 0.05	3.64	48	Intermediate
M1M-3	56.6 ± 2.0	10.4 ± 1.1	25.4 ± 2.4	7.6 ± 0.9			3.2 ± 0.4	0.77 ± 0.06	5.44	77	Si-poor
M1Q-8	57.5 ± 2.1	11.6 ± 1.3	15.8 ± 1.5	9.3 ± 1.0	5.8 ± 0.6		2.7 ± 0.3	0.74 ± 0.05	4.96	63	Si-poor
M1R-1b	57.8 ± 2.1	12.5 ± 1.4	19.3 ± 1.8	10.4 ± 1.2			2.4 ± 0.3	0.73 ± 0.05	4.62	65	Si-poor
M1R-1d	52.5 ± 1.9	12.2 ± 1.3	22.7 ± 2.1	12.6 ± 1.4			2.9 ± 0.4	0.90 ± 0.06	4.30	64	Si-poor
M1R-7	55.8 ± 2.0	10.7 ± 1.2	22.3 ± 2.1	11.3 ± 1.3			3.1 ± 0.4	0.79 ± 0.06	5.21	66	Si-poor
M1U-3	58.6 ± 2.1	9.7 ± 1.1	24.1 ± 2.3	7.6 ± 0.9			3.3 ± 0.4	0.71 ± 0.05	6.04	76	Si-poor
M1A3–3	62.8 ± 2.3	23.6 ± 2.6	7.0 ± 0.7	6.5 ± 0.7			0.6 ± 0.1	0.59 ± 0.05	2.66	52	Si-rich
M1K-4	61.0 ± 2.2	23.7 ± 2.6	10.0 ± 0.9	5.3 ± 0.6			0.6 ± 0.1	0.64 ± 0.05	2.57	65	Si-rich
M1R-1a	62.1 ± 2.2	23.8 ± 2.6	5.5 ± 0.5	8.5 ± 1.0			0.6 ± 0.1	0.61 ± 0.05	2.61	39	Si-rich
M1U-2b	61.5 ± 2.2	25.0 ± 2.8	3.9 ± 0.4	9.6 ± 1.1			0.5 ± 0.1	0.63 ± 0.05	2.46	29	Si-rich
M1D-2	66.9 ± 2.4	33.1 ± 3.6						0.49 ± 0.06	2.02		SiO_2
M1P-6	69.2 ± 2.5		9.9 ± 0.9			20.9 ± 5.2		0.45 ± 0.08			Spinel

Note. mg# = Mg/(Mg+Fe) * 100. Errors are 1σ.

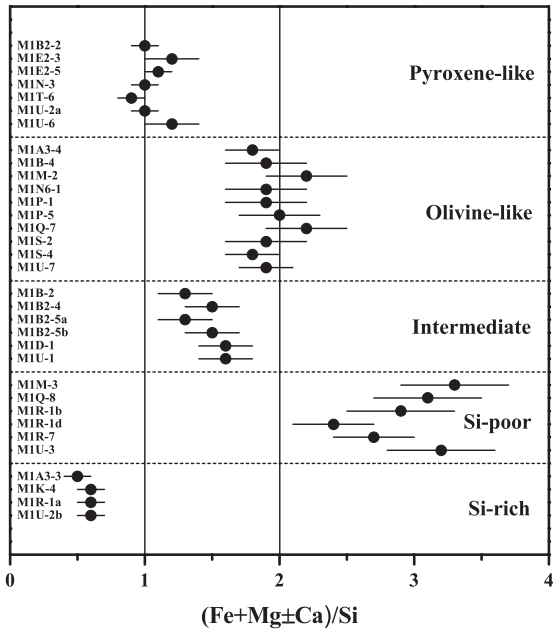

Figure 3. Plot of (Fe + Mg ± Ca)/Si ratios in presolar silicate grains from GRV 021710. Errors are 1σ (Table 3). See the text for details.

100, whereas grains with pyroxene-like compositions tend to be more Fe-rich (mg#s = 27−52).

Six silicate grains have (Fe+Mg+Ca)/Si ratios intermediate between pyroxene and olivine (1.3–1.6; Table 3 and Figure 3). We note that the cation/O and O/Si ratios of these grains are typically consistent with either olivine or pyroxene. Auger results from 141 olivine and pyroxene standards show that (Fe+Mg+Ca)/Si ratios have Gaussian distributions about the expected ratios of 2 and 1, with some overlap at intermediate compositions (Stadermann et al. 2009). Thus, some of our grains with such intermediate compositions may actually belong to either olivine-like or pyroxene-like categories. However, it is also important to note that other studies of presolar silicates have demonstrated that there is, in fact, a statistically significant population of grains with intermediate compositions (e.g., Floss & Stadermann 2009a; Bose et al. 2012). Five of these six intermediate grains have Mg-rich compositions (mg#s = 62−69), whereas the remaining one is slightly Fe-rich (mg# = 48). The remaining ten silicate grains with (Fe+Mg+Ca)/Si ratios that are either higher than olivine or lower than pyroxene are labeled as "Si-poor" and "Si-rich," respectively (Table 3 and Figure 3). All six Si-poor grains contain more Mg than Fe (mg#s = 63−77); one grain, M1Q-8, contains a small amount of

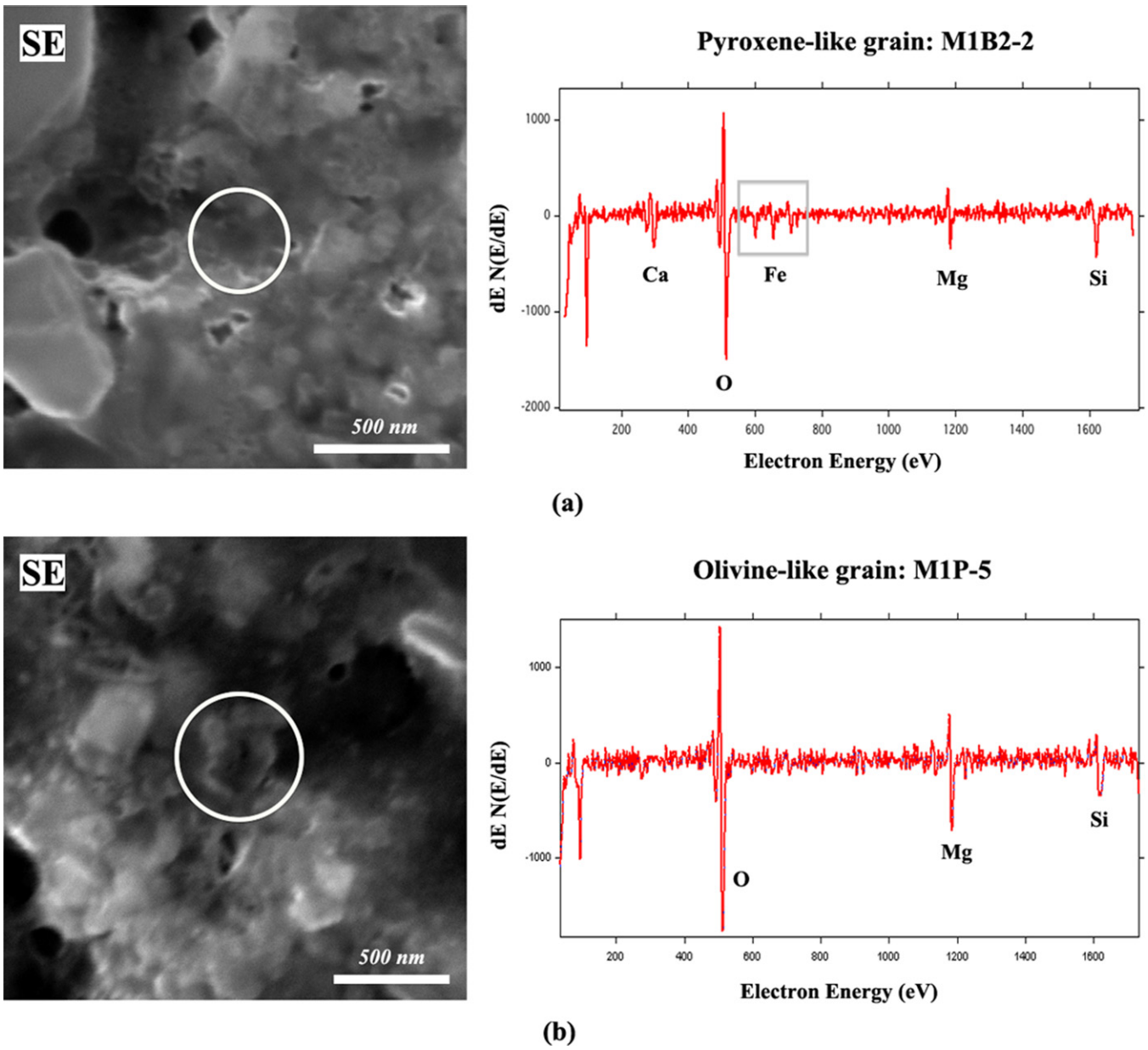

Figure 4. Secondary electron images and Auger spectra of Ca-bearing pyroxene-like grain M1B2–2 (a) and olivine-like grain M1P-5 (b). Both grains are circled in white.

(A color version of this figure is available in the online journal.)

Ca (5.8 ± 0.6 at%). Grain M1R-1b, with a (Fe+Mg+Ca)/Si ratio of 2.4, has a cation/O ratio consistent with olivine. As discussed above for the intermediate grains, this composition also could indicate an olivine-like grain. Of the four Si-rich grains, two grains, M1R-1a and M1U-2b, are Fe-rich, with mg#s of 39 and 29, respectively; Grain M1K-4 is relatively large (430 × 300 nm) and Mg-rich (mg# = 65); the final grain, M1A3–3, contains slightly more Mg than Fe (mg# = 52).

Only two oxide grains were identified. M1P-6 is ∼200 nm in diameter and has a composition identical with spinel ($MgAl_2O_4$). Figure 5(a) shows the Auger elemental maps of grain M1P-6, which clearly show enrichment of Al, O, and Mg. Grain M1D-2 is 300 × 260 nm in size and rich in Si and O (Figure 5(b)). Auger elemental quantification of this grain shows an O/Si ratio of ∼2, likely indicating an SiO_2 grain (Table 3).

3.3. C, N, Si Isotopic Analysis of Single SiC Grains

After Auger elemental analysis of the C-anomalous grains (in Section 3.2.1), seven SiC grains were selected for measurement of N and Si isotopes in grain mode. C, N, and Si isotopic compositions are listed in Table 4 and plotted in Figures 6 and 7. One of the measured SiC grains, M1R-6c, is highly ^{13}C-enriched ($^{12}C/^{13}C = 4.53 \pm 0.04$) and ^{15}N-enriched ($^{14}N/^{15}N = 30.1 \pm 0.7$). It shows depletion in ^{29}Si ($\delta^{29}Si = -377‰ \pm 12‰$) and excess in ^{30}Si ($\delta^{30}Si = 143‰ \pm 19‰$). The C, N, and Si isotopic composition of grain M1R-6c is similar to those thought to have originated from novae or supernovae (Amari et al. 2001; José et al. 2004; Nittler & Hoppe 2005). Another grain, labeled M4B-3c, has a $^{12}C/^{13}C$ ratio of 112 ± 1 and a slight depletion in ^{15}N ($^{14}N/^{15}N = 311 \pm 14$), and is classified as a type Y grain. Grain M1F-6c is ^{13}C-rich

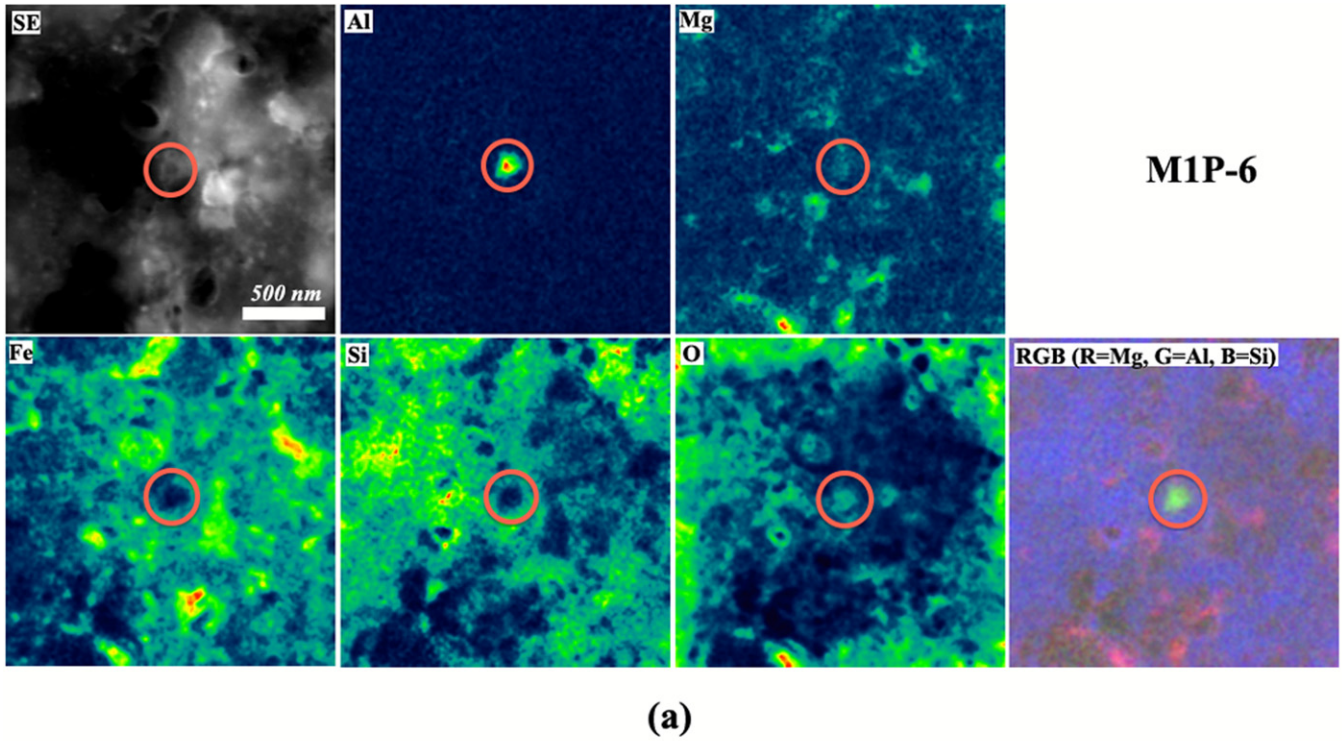

Figure 5. (a) Secondary electron images and Auger elemental maps of presolar spinel grain M1P-6 (circled in red). (b) Secondary electron images and Auger spectrum of silica grain M1D-2 (circled in white).

(A color version of this figure is available in the online journal.)

Table 4
C, N, and Si Isotopic Compositions (Grain Mode) of SiC Grains from GRV 021710

Grain	Size (nm)	$^{12}C/^{13}C$	$\delta^{13}C/^{12}C(‰)^a$	$^{14}N/^{15}N$	$\delta^{15}N/^{14}N(‰)^a$	$\delta^{29}Si/^{28}Si(‰)^a$	$\delta^{30}Si/^{28}Si(‰)^a$	Types[b]
M1R-6c	460 × 390	4.18 ± 0.03	20, 301 ± 142	30.1 ± 0.7	8040 ± 188	−377 ± 12	143 ± 19	Nova
M4B-3c	390 × 310	112 ± 1	−208 ± 2	311 ± 14	−124 ± 6	−9 ± 5	14 ± 6	Y
M1F-6c	650 × 400	57.3 ± 0.4	554 ± 4	660 ± 9	−588 ± 8	−10 ± 2	31 ± 2	Z
M1A2–6c	1060 × 800	43.8 ± 0.2	1034 ± 4	1164 ± 73	−766 ± 48	67 ± 5	75 ± 8	MS
M1T-3c	260 × 260	25.3 ± 0.6	2518 ± 64	476 ± 16	−428 ± 14	57 ± 6	53 ± 6	MS
M3J-4c	470 × 470	43.9 ± 0.4	1028 ± 8	1515 ± 90	−820 ± 49	58 ± 5	64 ± 6	MS
M3L-9c	390 × 230	60.3 ± 0.6	475 ± 5	319 ± 11	−148 ± 5	80 ± 6	49 ± 6	MS

Notes.

[a] Deviation from normal in parts per thousand: $(R_{meas}/R_{std} - 1) \times 1000$ (‰).

[b] MS: mainstream. Errors are 1σ.

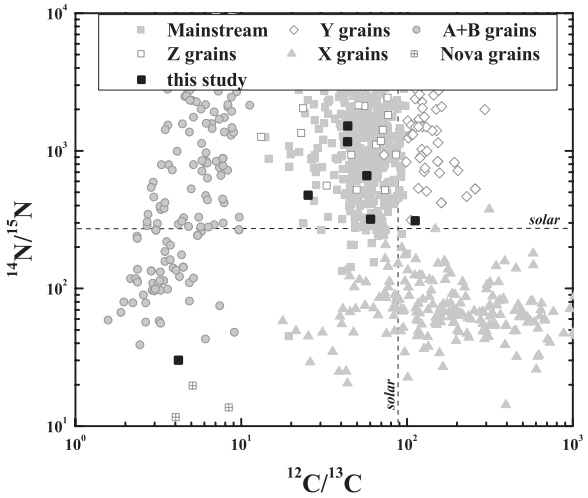

Figure 6. Plot of $^{12}C/^{13}C$ vs. $^{14}N/^{15}N$ ratios showing the compositions of seven SiC grains in GRV 021710. The dashed lines indicate solar values. The background data points (gray) are from the Presolar Grain Database at http://presolar.wustl.edu/~pgd/.

($^{12}C/^{13}C = 57.3 \pm 0.4$) and has a moderate depletion in ^{15}N ($^{14}N/^{15}N = 660 \pm 9$). The Si isotopic composition ($\delta^{29}Si = -10‰ \pm 2‰$; $\delta^{30}Si = 31‰ \pm 2‰$) of this grain indicates that it belongs to type Z. The remaining four grains are classified as mainstream SiC based on their C, N, and Si isotopic compositions.

4. DISCUSSION

4.1. Isotopic Signatures and Stellar Evolution

4.1.1. An SiC Grain from Nova?

The very low $^{12}C/^{13}C$, $^{14}N/^{15}N$, relatively large depletion in ^{29}Si, and excess in ^{30}Si make grain M1R-6c the most unusual of the SiC grains found in this study. Grains with such isotopic compositions have been considered to have an origin in the ejecta of classical novae (Amari et al. 2001). Classical novae are thermonuclear runaways caused by the hydrogen-rich matter accretion onto a white dwarf (WD) star surface from a close companion star. Astronomical observations suggest two categories for classical novae: CO novae and Ne novae (e.g., Gehrz et al. 1998). Typically, CO novae are explosions from C and O-rich WDs with mass $<1.1\,M_{\odot}$, while Ne (or ONe) novae are from WD stars rich in O and Ne from the burning of C ($M \geqslant 1.1\,M_{\odot}$). Amari et al. (2001) suggested that only ONe nova models can reproduce the isotopic compositions of possible nova grains, but the predicted anomalies are expected to be much larger than those observed in the grains, and material with close-to-solar isotopic compositions must be mixed into the nova ejecta to reproduce the grain compositions. Based on the nova models (Amari et al. 2001; José et al. 2004; Nittler & Hoppe 2005), the C, N, and Si isotopic compositions of our grain can be qualitatively explained and, like previous grains (Amari et al. 2001; Nittler & Hoppe 2005), the ^{29}Si depletions ($\delta^{29}Si = -377‰ \pm 12‰$) and ^{30}Si enrichments ($\delta^{30}Si = 143‰ \pm 19‰$) in grain M1R-6c require an origin in an ONe nova with a WD mass of $\geqslant 1.25\,M_{\odot}$. However, the origin of some nova grains becomes ambiguous if other isotopic systems such as Al, Ca, and Ti are considered. Nittler & Hoppe (2005) identified a nova candidate (SiC grain 151–4) on the basis of its C and N isotopic compositions. The Si isotopic composition ($\delta^{29}Si = -438‰ \pm 9‰$; $\delta^{30}Si = 510‰ \pm 18‰$) of this grain is very similar to that of our grain (Figure 7), but the ^{47}Ti excess and high $^{26}Al/^{27}Al$ ratio of grain 151–4 suggest that it might also be an SN grain. However, the Si isotopic signatures of these proposed nova grains have been considered diagnostic of ONe novae (Amari et al. 2001; José et al. 2004), and no single supernova zone is predicted to reproduce ^{30}Si enrichments and ^{29}Si depletions, as observed in some of the putative nova grains (Nittler & Hoppe 2005; Woosley & Weaver 1995; Rauscher et al. 2002). Nittler & Hoppe (2005) argued that mixtures of the ^{28}Si-rich Si/S zone and the ^{28}Si-poor O/Si zone could reproduce such isotopic compositions, suggesting that a nova origin is not the only explanation for this signature. In this case, it appears that the origin of grain M1R-6c is ambiguous without isotopic data for other minor elements. Unfortunately, our grain was completely consumed after the C–N–Si isotopic measurements, so no additional measurements could be made.

4.1.2. O-anomalous Grains: Groups and Distributions

The majority of the O-anomalous grains in GRV 021710 are Group 1 grains. If we take the three grains without ^{17}O data into account, the number of Group 1 grains is 89 out of 112. Group 1 grains are generally thought to have originated in low-to-intermediate-mass RG branch and AGB stars that

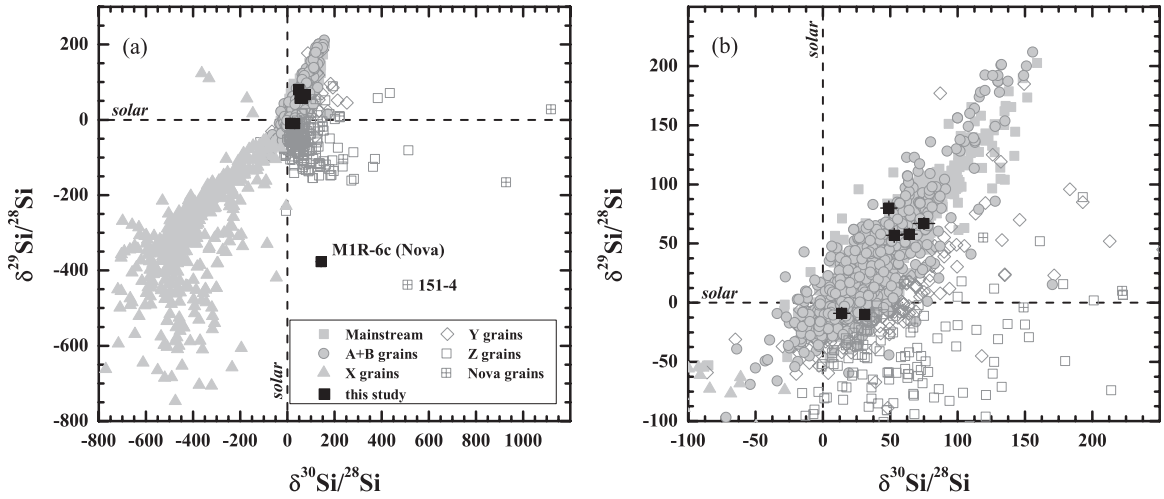

Figure 7. Silicon isotope ratio plots of seven SiC grains in GRV 021710. The dashed lines indicate solar values. The background data points are from the Presolar Grain Database at http://presolar.wustl.edu/~pgd/.

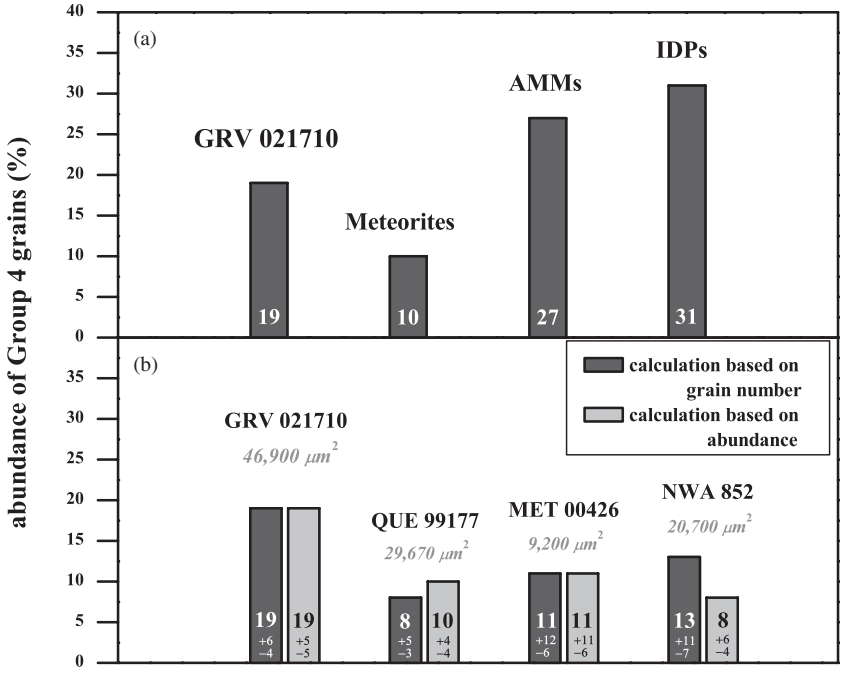

Figure 8. Histogram showing the abundances of Group 4 grains in GRV 021710 and: (a) different types of extraterrestrial materials; (b) three CR chondrites. For four CR chondrites, the total matrix areas analyzed for NanoSIMS imaging are also shown. Other data are from Haenecour et al. (2012), Floss & Stadermann (2009a), Nguyen et al. (2010), and Leitner et al. (2012). Errors are 1σ (Gehrels 1986).

have undergone the first and second dredge-ups to mix the CNO products of partial hydrogen burning into their envelopes (Nittler et al. 1997, 2008). Two grains with larger ^{18}O depletions ($^{18}O/^{16}O < 10^{-3}$) than typical Group 1 grains belong to Group 2, and originated in low-mass AGB stars ($M < 1.65\,M_{\odot}$) undergoing cool bottom processing (CBP; Wasserburg et al. 1995; Nollett et al. 2003). In CBP, extra mixing takes place when envelope material is circulated down to regions hot enough for hydrogen burning nuclear reactions, which rapidly destroy ^{18}O, via the reaction ^{18}O (p, α) ^{15}N. Nguyen et al. (2007) showed that, with NanoSIMS ion imaging, the isotopic signatures of presolar grains are diluted by the surrounding isotopically normal materials. The compositions of grains with isotopic depletions are more diluted than grains with isotopic excesses. Thus, the intrinsic compositions of our Group 2 grains are probably more ^{18}O depleted than they appear. Likewise, some of our Group 1 grains with relatively low $^{18}O/^{16}O$ ratios (close to 10^{-3}) may actually belong to Group 2.

Group 4 grains (21 grains) are the second most abundant O-anomalous group in this study. Note that one grain, M6C-4, with a small ^{18}O enrichment ($^{18}O/^{16}O = 2.29 \times 10^{-3}$), but much larger ^{17}O enrichment ($^{17}O/^{16}O = 14.1 \times 10^{-4}$), has been classified as a Group 1 grain. Oxygen-17 data for M5A-14 a and M5A-15 are unavailable, so we only discuss the remaining 19 grains here. Among these grains, most of them have ^{17}O enrichments similar in magnitude to the ^{18}O enrichments (Figure 1). Nittler (2007) suggested that such O isotopic signatures could be reproduced by a single material jet from the inner ^{16}O-rich zone passing through the outer ^{17,18}O-rich layers and mixing with the ^{17,18}O-rich material and that such grains might have an origin in a single Type II SN.

The abundance of Group 4 grains in GRV 021710 (~19%) is relatively high compared to other primitive meteorites (Figure 8(a)). Haenecour et al. (2012) estimated average abundances of Group 4 grains of 10%, 27%, and 31%, respectively, for meteorites, Antarctic micrometeorites (AMMs), and IDPs. These observations may imply a heterogeneous distribution of supernova presolar grains among different types of extraterrestrial materials. The Group 4 grain abundance in GRV 021710 is significantly higher than the overall abundance of other primitive meteorites, but is comparable to the abundances observed in AMMs and IDPs (Figure 8(a)). Figure 8 compares different abundances of Group 4 grains in the CR chondrites. As shown in Figure 8(b), the abundances of the CR chondrites were calculated based on both the numbers of grains and using the actual abundances of Group 4 grains relative to all the O-anomalous grains. In both cases, the abundance of Group 4 grains is higher in GRV 021710 than in the other CR chondrites. Although the differences are not resolvable on a statistical basis, the trend nevertheless suggests that a heterogeneous distribution of Group 4 grains may also be present in the CR group (Figure 8(b)). Based on the numerical simulations performed by Vanhala & Boss (2000), shock waves caused by nearby stellar explosions could lead to temporal and spatial heterogeneities in the abundances of radioactivities by injecting freshly synthesized radioactivities into the early solar system. Such a process could also result in heterogeneities in the abundances of elements and isotopes. If most Group 4 grains indeed come from a single SNII (Nittler 2007), such a heterogeneous distribution of Group 4 grains could be due to different proportions of supernova grains injected into different parts of the early solar nebula, or at different times during formation of the solar system.

Another possible explanation for the heterogeneous distribution of Group 4 grains could be size sorting in the nebula. Previous investigations of the acid residue of Qingzhen (EH3) chondrite indicated that the abundance of presolar SiC X grains in the smaller size fraction (0.1−0.4 μm, ~2%) is about eight times higher than those in the larger size fraction (0.4−2 μm, <0.25%; Lin et al. 2002, 2011). Since mainstream SiC grains and type X SiC grains are thought to have originated in different stellar sources (AGB stars and supernovae, respectively), these authors suggested that different stellar environments could

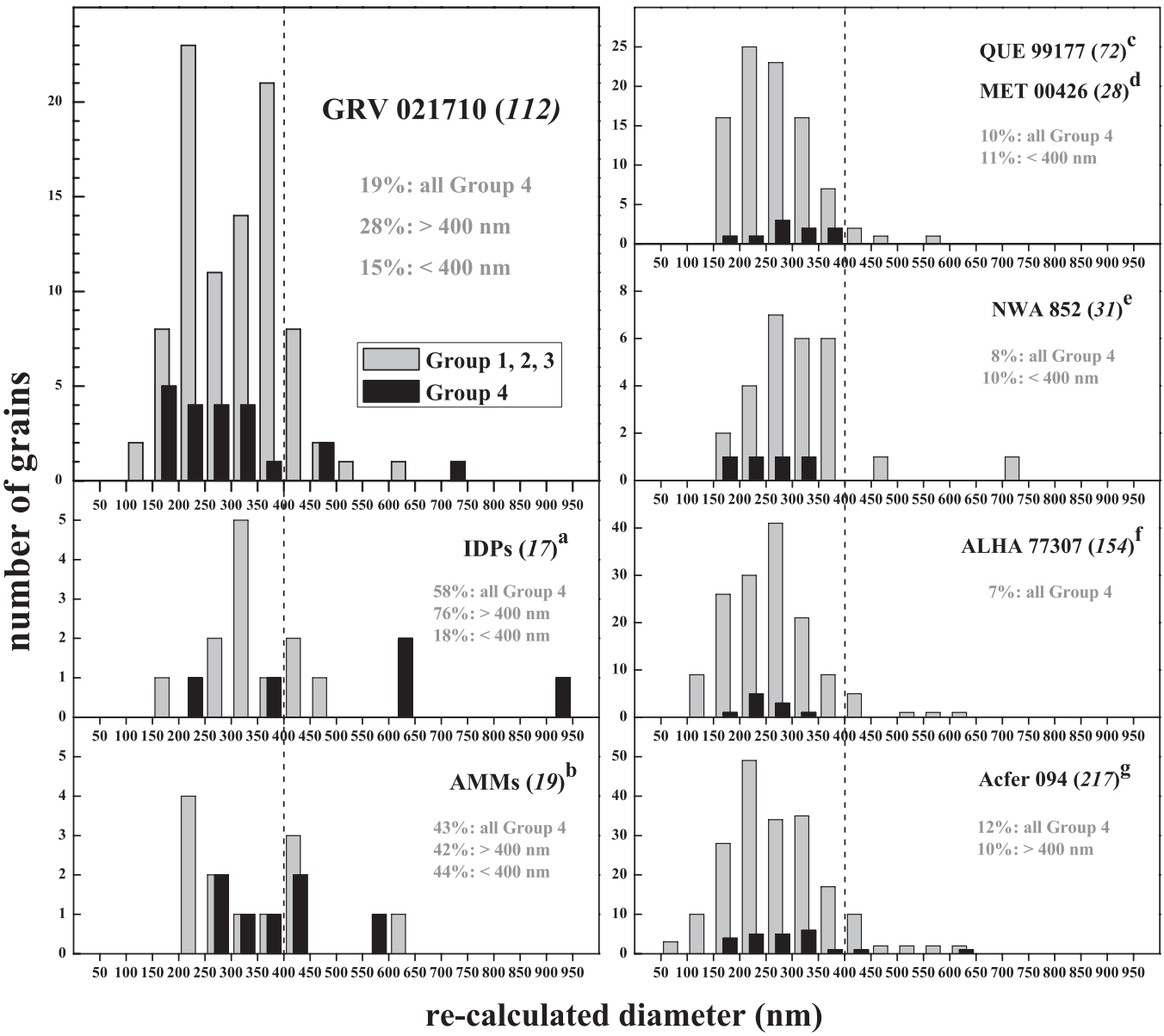

Figure 9. Histogram showing the size distributions of the presolar O-anomalous grains in primitive exterrestrial materials. The dashed line is located at 400 nm. The abundances of Group 4 grains (%) are shown in gray text. The numbers in parentheses after the sample name indicate the number of O-anomalous grains identified from each sample. The number for GRV 021710 is from this study, others are from the literature: [a] Messenger et al. (2003), Floss et al. (2006), Stadermann et al. (2006); [b] Yada et al. (2008); [c, d] Floss & Stadermann (2009a), Nguyen et al. (2010); [e] Leitner et al. (2012); [f] Nguyen et al. (2010), Bose et al. (2012); [g] Nguyen & Zinner (2004), Floss et al. (2008), Vollmer et al. (2009b), Bose et al. (2010).

result in the distinct size distributions observed in SiC grain types. The average sizes of presolar SiC grains from supernovae might be smaller than those of mainstream grains. Group 4 grains also have origins in Type II SNe (Nittler et al. 2008), and therefore in order to explore the possibility that Group 4 grains have been affected by size sorting, we compared the grain sizes among different grain groups and different primitive exterrestrial materials (Figure 9). Grain size data of other primitive exterrestrial materials are from the literature. Since grain sizes determined using NanoSIMS ion images are generally larger than those from Auger SE images, we preferentially use the grain sizes determined using Auger SE images. For grains in which only NanoSIMS data are available, we applied a correction to the grain sizes in order to make a more meaningful comparison. This was done by comparing grain sizes from both NanoSIMS and Auger data for over 100 grains in which both were available; the results showed that the NanoSIMS determinations were typically 20%–30% larger. Overall, the Group 4 grains have size ranges similar to those of the Group 1−3 grains, with no significant size-dependent distributions such as those observed in type X SiC grains. Thus, the heterogeneous abundances of Group 4 grains observed in different types of primitive exterrestrial materials are not related to grain size, leaving supernova injection as the more likely possibility.

4.2. Chemical Compositions of O-anomalous Grains

4.2.1. Presolar Silicates: Overall Picture

Based on the Auger elemental results (Table 3), about half of our presolar silicate grains (14 out of 33) have stoichiometric compositions consistent with either olivine or pyroxene

(three grains with non-stoichiometric cation/O and Si/O ratios are not included; see Section 3.2.2.). However, we cannot tell whether these grains are crystalline or amorphous based only on Auger spectroscopy. Spectral observations show the presence of both crystalline and amorphous silicates around oxygen-rich AGB stars (Waters et al. 1996; Demyk et al. 2001). Molster et al. (2002) showed that for spectra dominated by crystalline forsterite and enstatite, enstatite is more abundant for most stellar sources. On the other hand, the broad features of amorphous silicates are better explained by primarily olivine compositions, with pyroxene compositions representing $\leqslant$10% of the total mass of the amorphous silicates (Demyk et al. 2000). In this study, seven grains are olivine-like grains and seven grains are pyroxene-like, which is inconsistent with that expected from either predominantly crystalline or predominantly amorphous sources. Among presolar silicate grains analyzed using TEM to date, only a small fraction have crystalline structures (Messenger et al. 2005; Stroud et al. 2009; Vollmer et al. 2007, 2009a), with one grain reported as $MgSiO_3$ perovskite (Vollmer et al. 2007). Most of the presolar silicate grains analyzed using TEM have non-stoichiometric compositions and are amorphous to weakly nanocrystalline (Nguyen et al. 2007, 2010; Vollmer et al. 2009a). These results suggest that both crystalline and amorphous grains may be part of our grain inventory. In addition, six of our presolar silicate grains are classified as intermediate grains based on their (Fe + Mg + Ca)/Si ratios (1.3−1.6; Table 3). The average O/Si ratio (3.54) of these intermediate grains is consistent with the O/Si ratio of ∼3.5 of amorphous silicates in the ISM (Min et al. 2007). These authors also predicted Mg-rich compositions (Min et al. 2007), which is also consistent with the chemical compositions of most of our intermediate grains (mg#s = 62−69; Table 3). Therefore, it is possible that most of our intermediate silicate grains are amorphous.

Four grains are Si-rich, with (Fe + Mg + Ca)/Si ratios (0.5−0.6) lower than those of pyroxene (Table 3). Of these grains, two grains are Fe-rich, with mg#s of 39 and 29 respectively, whereas the remaining two grains are Mg-rich (mg#s = 52−65). Si-rich grains may originate in kinetically fractionating systems, in which the nucleation of Fe onto forsterite inhibits the equilibration of forsterite with Si-rich gas to form enstatite, allowing Si-rich grains to form (Nagahara & Ozawa 2009). Six presolar silicate grains are Si-poor and have (Fe + Mg + Ca)/Si ratios higher than olivine (2.4−3.3; Table 3). All of these grains are Mg-rich and have mg#s from 63 to 77, which is similar to the results from the CR3 chondrites QUE 99177 and MET 00426 (Floss & Stadermann 2009a). As noted by Floss & Stadermann (2009a), such non-stoichiometric compositions, with (Fe + Mg + Ca)/Si ratios around 3.0, are intermediate between olivine and magnesiowüstite (the solid solution series that consists of periclase (MgO) and wüstite (FeO) end members). Both theoretical calculations and laboratory studies suggest that magnesiowüstite can condense under non-equilibrium conditions, particularly at high Mg/Si ratios, in the outflows of oxygen-rich AGB stars (Gail & Sedlmayr 1999; Nuth et al. 2000; Ferrarotti & Gail 2001). More detailed calculations by Ferrarotti & Gail (2003) show that magnesiowüstite is likely to condense in the stellar outflows with low mass-loss rates, while its condensation is inhibited by the early condensation of silicates at higher mass-loss rates. Therefore, presolar silicates with Si-poor compositions may condense as non-stoichiometric mixtures of Mg-rich oxides and silicates in stellar environments with rapidly changing conditions.

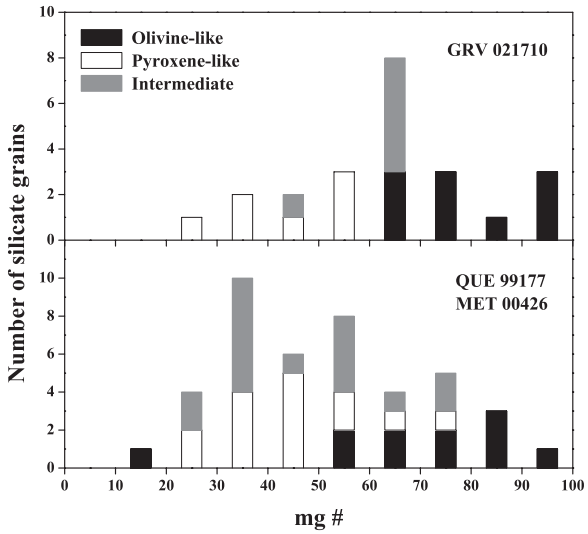

Figure 10. Histogram showing the mg#s of presolar silicate grains in GRV 021710, compared with those in the CR3 chondrites QUE 99177 and MET 00426 (Floss & Stadermann 2009a); mg# = Mg/(Mg + Fe) × 100.

4.2.2. Fe Contents in Presolar Silicate Grains

Figure 10 shows the distribution of mg#s for olivine-like, pyroxene-like grains, and grains with intermediate compositions, as well as grains from the CR3 chondrites QUE 99177 and MET 00426 (Floss & Stadermann 2009a). All olivine-like grains in our inventory are distinctly Mg-rich, with mg#s greater than 50. Three grains have compositions consistent with nearly pure forsterite (mg# = 100; Table 3 and Figure 10). In contrast, pyroxene-like grains tend to be more Fe-rich; all but two grains have mg#s lower than 50 (Table 3 and Figure 10). Mg-rich grains also dominate among the presolar silicates with non-stoichiometric compositions in GRV 021710; only one intermediate grain and two Si-rich grains are Fe-rich (Table 3 and Figure 10). This distribution of mg#s is quite different from the relatively Fe-rich trends observed in Acfer 094 (Nguyen & Zinner 2004; Nguyen et al. 2007; Vollmer et al. 2009b; Bose et al. 2010) and the CR3 chondrites, QUE 99177 and MET 00426 (Floss & Stadermann 2009a). As we discussed before, astronomical observations and modeling calculations predict that both crystalline and amorphous silicate grains should be Mg-rich, with mg#s >90 (Molster et al. 2002; Demyk et al. 2000; Min et al. 2007). Furthermore, equilibrium condensation models predict that the first silicate phases condensed in high-temperature O-rich stellar ejecta are expected to have essentially pure Mg-rich compositions (Lodders & Fegley 1999; Ferrarotti & Gail 2001; Gail 2003). As temperatures decrease, Fe contents are expected to increase during equilibrium condensation (Lodders & Fegley 1999; Gail 2003). However, in environments such as circumstellar shells with low temperatures, cation diffusion is so slow that equilibration is essentially prohibited (e.g., Gail 2003). Three of our grains exhibit stoichiometric compositions of forsterite; however, most of our Mg-rich grains do not have mg#s as high as those predicted by astronomical observations and modeling calculations. Condensation under non-equilibrium environments can also enhance the Fe contents of silicate minerals, and dust in stellar outflows is expected to condense in a rapidly cooling environment, in which equilibrium may not be maintained. However, laboratory experiments for the non-equilibrium con-

densation of silicates show that either MgSiO or FeSiO end-member compositions can be produced from Mg, Fe, and SiO vapors, but mixed MgFeSiO compositions do not form (Rietmeijer et al. 1999). These results suggest that three grains with forsterite compositions found in this study may have condensed under such circumstellar environments. However, for the vast majority of our presolar silicates with mixed ferromagnesian compositions, it is difficult to evaluate whether primary condensation may have contributed to the Fe enrichment seen in the presolar silicate grains.

Nguyen & Zinner (2004) initially suggested that secondary processes, including thermal metamorphism and aqueous alteration, could also introduce Fe into presolar silicate grains. Diffusion of Fe during thermal metamorphism can increase the Fe contents of silicates that were originally Mg-rich (Jones & Rubie 1991). Generally, such processes can occur in the solar nebula, as well as in the parent bodies of meteorites. Previous work on the matrix of GRV 021710 found no evidence of significant thermal metamorphism (Miao et al. 2007). NanoSIMS ion imaging for S isotopes shows that the matrix of GRV 021710 contains abundant submicron-sized (∼200 nm) sulfide grains, which are similar to those observed in the CR3 chondrites QUE 99177 and MET 00426 by Abreu & Brearley (2010). These authors demonstrated that S (Fe, Ni-sulfides) is distributed homogeneously through the matrix in low petrologic type 3 chondrites, but after limited thermal metamorphism, it occurs as coarser-grained sulfide grains. This suggests that the GRV 021710 may have escaped any significant effects of thermal metamorphism. Most recently, Floss & Stadermann (2012) found that many grains in the ungrouped carbonaceous chondrite Adelaide have Fe-rich rims that seem to suggest infusion of Fe into the Mg-rich grains from the surrounding Fe-rich matrix material, resulting in elevated Fe content in these grains. However, such Fe-rich rims are not present around our grains. Moreover, since olivine is more sensitive to thermal metamorphism and has faster cation diffusion rates than pyroxene (e.g., Freer 1981; Mikouchi et al. 2003), the diffusion of Fe would lead to more Fe-rich olivines than pyroxenes. In contrast, our silicate grains, as well as those from the primitive CR3 chondrites, show more Fe-rich pyroxenes than olivines (Table 3 and Figure 10; Floss & Stadermann 2009a). Thus, it seems that thermal metamorphism on the meteorite parent body is not responsible for the Fe enrichments in some presolar silicate grains in GRV 021710. On the other hand, compared to the pristine CR3 chondrites, QUE 99177 and MET 00426, which appear to have experienced only little hydration (Floss & Stadermann 2009a; Abreu & Brearley 2010), the presolar silicates in GRV 021710 show lower Fe contents. Abreu & Brearley (2008) noted that Fe might be leached out of silicate grains to form magnetite and Fe oxides during aqueous alteration. Thus, aqueous alteration could account for the fact that the Fe abundances in our grains are lower than those of the CR3 chondrites. However, this would indicate that the original Fe contents of the grains were even higher than those currently observed.

In summary, although our silicate grains are more Mg-rich than those in other CR3 chondrites, the Fe contents in some grains are still significantly higher than the astronomical observations and the predictions of the modeling calculations. It appears that both the thermal metamorphism and the aqueous alteration that commonly occur on meteorite parent bodies are not responsible for the elevated Fe contents in some of our presolar silicate grains, requiring a primary origin for the Fe that is present in the grains.

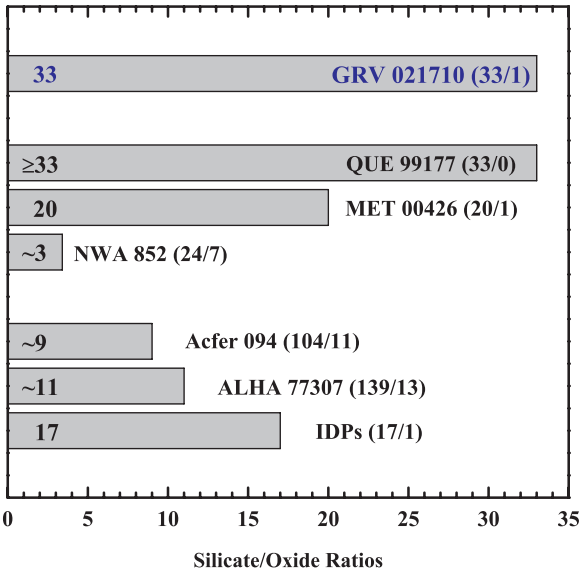

Figure 11. Bar graph showing the presolar silicate/oxide ratios in primitive meteorites and IDPs. The numbers in parentheses after the meteorite name indicate the number of silicates and oxides identified from each sample (silicates/oxides). Data for GRV 021710 are from this study; other data are from Bose et al. (2010), Bose et al. (2012), Floss & Stadermann (2009a), Messenger et al. (2003, 2005), Nguyen et al. (2010), Vollmer et al. (2009b), Stadermann et al. (2006), and Leitner et al. (2012).

(A color version of this figure is available in the online journal.)

4.2.3. Presolar Oxide Grains and Silicate/Oxide Ratios

Two presolar oxide grains were found in our inventory (Table 3). One of these, M1P-6, is a Group 4 grain with correlated ^{17}O and ^{18}O enrichments (Table 2), suggesting an origin in a Type II SN. This grain has a nearly stoichiometric composition of spinel ($MgAl_2O_4$). The other oxide grain (M1D-2) is also a Group 4 grain, with moderate excess in ^{18}O and close-to-solar $^{17}O/^{16}O$ ratio (Table 2). This grain contains only Si and O peaks in the Auger spectrum and has a stoichiometric composition consistent with SiO_2 (Table 3 and Figure 5(b)). The origin of this grain will be discussed in more detail in a separate publication.

Floss & Stadermann (2009a) suggested that silicate/oxide ratios could reflect the degree of secondary processing experienced by the meteorite parent bodies presolar oxide are refractory phases, such as corundum, spinel, and hibonite, and are more resistant to parent body processing than silicates. For the following discussion, we only consider spinel M1P-6 as an oxide grain. Figure 11 shows the presolar silicate/oxide ratios for CR chondrites, as well as other primitive meteorites and IDPs. All ratios were calculated on the basis of the numbers of the silicate and oxide grains. Note that, for some meteorites (such as Acfer 094), NanoSIMS ion images were also used for the identification of silicate grains on the basis of correlated $^{24}Mg^{16}O$ and ^{28}Si signals in some studies (e.g., Nguyen & Zinner 2004). Here, we only use the data that we have obtained from Auger spectroscopy, because mineral phase identification based on NanoSIMS secondary ion yields may lead to misidentifications and subsequent errors in the silicate/oxide ratios (Bose et al. 2010). As shown in Figure 11, the CR3 chondrites, QUE 99177 and MET 00426, have high silicate/oxide ratios (⩾20) (Floss & Stadermann 2009a). The silicate/oxide ratio for the O-anomalous grains in GRV 021710 is 33, close to the highest value of QUE 99177 (⩾33). In contrast,

CR2 chondrite NWA 852 has the lowest silicate/oxide ratio (∼3) among all presolar grain-rich meteorites (Leitner et al. 2012). We also calculated silicate/oxide ratios of about 9 and 11 respectively for two well-studied carbonaceous chondrites, Acfer 094 and ALHA 77307 (Vollmer et al. 2009b; Bose et al. 2010, 2012; Nguyen et al. 2010). Leitner et al. (2012) also calculated silicate/oxide ratios based on the relative abundances of presolar silicate and oxide grains (see his Figure 11). Their calculation shows that the CR3 chondrites, the CO3 chondrite ALHA 77307, and IDPs have presolar silicate/oxide ratios ranging from 16 to 27, whereas the ratio of CR2 chondrite NWA 852 is only ∼2. If we recalculate the ratio based on the abundance of presolar grains, the result of GRV 021710 would be >50, which is even higher than those of the CR3 chondrites and the IDPs. Since silicate grains are less resistant to thermal metamorphism and aqueous alteration than oxides (Huss et al. 2003), lower silicate/oxide ratios are thought to represent matrix materials that have undergone more processing, implying that parent body alteration has destroyed a significant amount of the silicate grains in NWA 852, the meteorite with the lowest silicate/oxide ratio. In contrast, higher silicate/oxide ratios, such as those observed in GRV 021710, the CR3 chondrites, the CO3 chondrite ALHA 77307, and IDPs, should come much closer to represent the original proportions of presolar silicates and oxides in the parent molecular cloud of the solar nebula. Most of the presolar O-anomalous grains originated from low-to-intermediate-mass AGB stars (Zinner 2007). Leitner et al. (2012) calculated a silicate/oxide ratio of 23 for dust from AGB stars by assuming that all Si from AGB stars condenses into silicate, while all Al condenses into oxide dust. This ratio is consistent with the ratios determined for primitive CR3 chondrites, IDPs, and GRV 021710. Although the small numbers of the presolar oxides grains in these samples introduce large uncertainties to the presolar silicate/oxide ratios, the overall trend of high presolar silicate/oxide ratios suggests a relatively low degree of secondary processing experienced by the parent bodies of these meteorites, including GRV 021710. As discussed before, the matrix of GRV 021710 contains abundant nanosulfide grains, suggesting that the GRV 021710 parent body may have barely experienced any significant effects of thermal or aqueous metamorphism. Scanning electron microscopy (SEM) imaging shows that the matrix of GRV 021710 contains only low abundances of magnetite and calcite, also suggesting a low degree of aqueous alteration. We have not used TEM to survey the phyllosilicates abundance, but all of the evidence suggests that GRV 021710 is more primitive than typical CR2 chondrites and that a CR3 classification may be more appropriate.

4.3. Presolar Grain Abundances

The 35 C-anomalous grains found in this study result in a matrix-normalized abundance of 235 ± 40 ppm, which is similar, within analytical uncertainties, to the abundances of 215 ± 35 and 175 ± 30 ppm in the CR3 chondrites QUE 99177 and MET 00426 (Floss & Stadermann 2009b). The calculated abundance of SiC grains in GRV 021710 is 182 ± 33 ppm, which is about a factor of two higher than the average SiC abundance (65 ± 10 ppm) in QUE 99177 and MET 00426 (Floss & Stadermann 2009b), and is similar to the SiC abundance in NWA 852 of 160 ± 57 ppm (Leitner et al. 2012). GRV 021710 also contains abundant C-anomalous carbonaceous grains, with a calculated abundance of 35 ± 14 ppm.

The overall O-anomalous grain abundance of 189 ± 18 ppm is comparable to that of the CR3 chondrites QUE 99177 and MET 00426 (Floss & Stadermann 2009a). We did not find any heterogeneity of the grain distribution, as has been observed in other CR chondrites (Floss & Stadermann 2009a; Leitner et al. 2012), and in other carbonaceous chondrites (Zhao et al. 2011a). The 112 O-anomalous grains were identified in five different matrix areas. The abundances of the O-anomalous grains in the five matrix areas range from 175 to 200 ppm. Results from CR3 chondrites QUE 99177 and MET 00426 show that the distribution of presolar O-anomalous grains in these two meteorites is heterogeneous among different matrix areas (300 ppm in 5400 μm^2 vs. 90 ppm in 3100 μm^2; Floss & Stadermann 2009a). These authors suggested that matrix material, with higher presolar grain abundances, might have undergone less secondary processing than other matrix areas with lower presolar grain abundances in the solar nebula before accretion into the meteorite parent body, or possibly accreted from a presolar grain-rich region in the solar nebula. The ungrouped type-3 carbonaceous chondrite Ningqiang also exhibits such heterogeneity, with two areas having extremely different abundances of presolar O-anomalous grains (256 ppm in 10,800 μm^2 vs. ∼6 ppm in 9000 μm^2; Zhao et al. 2011a). Scanning electron microscopy imaging shows that, in Ningqiang, the presolar grain-rich matrix is less abundant in Fe–Ni metal and sulfide, and has a smaller average grain size than the other presolar grain-poor area. Zhao et al. (2011a) suggested that the presolar grain-poor matrix area might have been affected by some thermal metamorphism in the nebula in a different region, which had relatively larger grains and contained more opaque minerals. The matrix of GRV 021710 appears relatively homogeneous. The high abundances of presolar grains in GRV 021710 provide additional evidence that GRV 021710 may be a CR3 chondrite.

As the tenth most abundant element in the universe (Lodders 2003), S is present in massive stars and was ejected into the ISM when stars exploded, such as Type II SNe (Timmes et al. 1995). Sulfur molecules are observed in the ISM and in circumstellar shells around low-to-intermediate-mass stars (Tielens 2005; Kahane et al. 1988) and were predicted by molecule formation models of SNeII ejecta (Cherchneff & Dwek 2009). Although S anomalies that originated in SN have been found in SiC grains (Hoppe et al. 2012; Xu et al. 2012), no presolar sulfide grains have been identified yet. Keller & Rahman (2011) suggested that lack of presolar sulfide might due to destruction processes in the ISM, e.g., sputtering out by high energy particles and/or X-ray from passage of SN-generated shock waves (Jones & Nuth 2011). Simulation experiments have demonstrated that the sputtering rate of FeS is about four times faster than silicates (Keller & Rahman 2011). In other words, the lifetime of sulfide grains is much shorter than that of silicates. Hence, the absence of presolar sulfides might be due to their nearly complete destruction before incorporation into the meteorite parent body. Jenkins (2009) predicted a silicate/sulfide ratio of 8 on the basis of the S/Si ratio of ∼0.5 in the diffuse ISM. GRV 021710 has a matrix normalized abundance of ∼165 ppm for presolar silicates and, thus, we would expect an abundance of presolar sulfide grains of ∼20 ppm in this meteorite if sulfides are destroyed four times faster than silicates. However, we have determined an upper limit of ∼2 ppm for presolar sulfides, significantly lower even than the prediction taking into consideration the faster sputtering rate of sulfide.

5. CONCLUSIONS

The CR chondrite GRV 021710 contains abundant presolar C- and O-anomalous grains, with 236 ± 40 and 189 ±

18 ppm, respectively. It is one of the most presolar grain-rich primordial meteorites. Based on the isotopic and/or elemental compositions of these grains, we can summarize the following conclusions.

1. The abundance of presolar SiC grains (182 ± 34 ppm) in GRV 021710 is the highest observed in a primitive meteorite so far. Most of the SiC grains (∼80%) in our inventory are mainstream grains. Two Y grains and one Z grain were also identified. The final grain has a very low $^{12}C/^{13}C$, $^{14}N/^{15}N$, and relatively large depletion in ^{29}Si and excess in ^{30}Si, suggesting an origin in a nova or supernova.
2. The O isotopic compositions of 112 O-anomalous grains in GRV 021710 span three groups of presolar silicate/oxide grains, with the majority having origins in low-to-intermediate-mass RG and AGB stars, as expected. Two grains are defined as Group 2, and probably originated in low-mass AGB stars undergoing CBP. Twenty-one grains are Group 4 grains and originated in Type II supernovae.
3. The abundance of Group 4 grains in GRV 021710 is the highest value observed to date in meteorites, and is similar to those of the AMMs and the IDPs, suggesting a heterogeneous distribution of Group 4 grains in the solar nebula. The parent body of GRV 021710 might have formed at a location in the solar nebula (or time during the solar system formation) that incorporated a relatively large proportion of supernova materials.
4. Auger elemental results of 35 O-anomalous grains show that 33 grains are ferromagnesian silicates (165 ± 29 ppm). Most of these silicate grains are more Mg-rich than those observed in other primitive meteorites; however, the Fe contents in some grains are still significantly higher than the astronomical observations and the predictions of the modeling calculations. Secondary processes seem not to be responsible for such unexpected Fe contents in these grains, and a primary origin would be considered.
5. Two presolar oxide grains (9 ± 6 ppm) were identified. The silicate/oxide ratio of GRV 021710 is comparable with those of unaltered CR3 chondrites and primitive IDPs, and may reflect the initial proportions of presolar silicates and oxides in the parent molecular cloud of the solar nebula.
6. No S-anomalous grains were found in this study, which results in an upper limit of ∼2 ppm for the presolar sulfide grains in GRV 021710. This upper limit is significantly lower than the predicted value, even with consideration of preferential destruction of sulfide grains in the ISM.
7. Evidence from the unusually high presolar grain abundances, mg#s, and silicate/oxide ratios, as well as SEM and Auger observations for petrologic signatures of the matrix, imply that GRV 021710 is a one of the most pristine CR chondrites and a petrologic type 3 classification may be more appropriate.

We thank Tim Smolar and Eric Inazaki for maintenance of the WashU NanoSIMS and Auger Nanoprobe, and Jialong Hao and Jianchao Zhang for their technical support of the IGGCAS NanoSIMS. We also thank an anonymous reviewer for detailed and constructive comments, which helped improve the paper. The thin section of GRV 021710 is provided by the Polar Research Institute of China. This work is supported by the Natural Science Foundation of China (40830421) and NASA grant (NNX10AH43G).

REFERENCES

Abreu, N., & Brearley, A. 2008, in 38th Lunar Planet. Sci. Conf., ed. S. J. Mackwell (League City, TX: LPI), abstract 2013
Abreu, N., & Brearley, A. 2010, GeCoA, 74, 1146
Amari, S., Gao, X., Nittler, L. R., et al. 2001, ApJ, 551, 1065
Bose, M., Floss, C., & Stadermann, F. J. 2010, ApJ, 717, 1624
Bose, M., Floss, C., Stadermann, F. J., Stroud, R. M., & Speck, A. K. 2012, GeCoA, 93, 77
Cherchneff, I., & Dwek, E. 2009, ApJ, 703, 642
Demyk, K., Dartois, E., Wiesemeyer, H., Jones, A. P., & d'Hendecourt, L. 2000, A&A, 364, 170
Demyk, K., Carrez, P., Leroux, H., et al. 2001, A&A, 368, L38
Ferrarotti, A. S., & Gail, H.-P. 2001, A&A, 371, 133
Ferrarotti, A. S., & Gail, H.-P. 2003, A&A, 398, 1039
Floss, C., & Stadermann, F. J. 2005, in 36th Lunar Planet. Sci. Conf., ed. S. J. Mackwell (League City, TX: LPI), abstract 1390
Floss, C., & Stadermann, F. J. 2009a, GeCoA, 73, 2415
Floss, C., & Stadermann, F. J. 2009b, ApJ, 697, 1242
Floss, C., & Stadermann, F. J. 2012, M&PS, 47, 992
Floss, C., Stadermann, F. J., & Bose, M. 2008, ApJ, 672, 1266
Floss, C., Stadermann, F. J., Bradley, J. P., et al. 2006, GeCoA, 70, 2371
Freer, R. 1981, CoMP, 76, 440
Gail, H.-P. 2003, in Astromineralogy, ed. T. Henning (Berlin: Springer), 55
Gail, H.-P., & Sedlmayr, E. 1999, A&A, 347, 594
Gehrels, N. 1986, ApJ, 303, 336
Gehrz, R. D., Truran, J. W., Williams, R. E., & Starrfield, S. 1998, PASP, 110, 3
Haenecour, P., Floss, C., & Yada, T. 2012, M&PSA, 47, 5220
Hoppe, P., Fujiya, W., & Zinner, E. 2012, ApJL, 745, L26
Huss, G. R., Meshik, A. P., Smith, J. B., & Hohenberg, C. M. 2003, GeCoA, 67, 4823
Jenkins, E. B. 2009, ApJ, 700, 1299
Jones, A. P., & Nuth, J. A. 2011, A&A, 530, A44
Jones, R. H., & Rubie, D. C. 1991, EPSL, 106, 73
José, J., Hernanz, M., Amari, S., Lodders, K., & Zinner, E. 2004, ApJ, 612, 414
Kahane, C., Gomez-Gonzalez, J., Cernicharo, J., & Geuelin, M. 1988, A&A, 190, 167
Keller, L. P., & Rahman, Z. 2011, M&PSA, 46, A121
Krot, A. N., Meibom, A., Weisberg, M. K., & Keil, K. 2002, M&PS, 37, 1451
Leitner, J., Vollmer, C., Hoppe, P., & Zipfel, J. 2012, ApJ, 745, 38
Lin, Y., Amari, S., & Pravdivtseva, O. 2002, ApJ, 575, 257
Lin, Y., Hoppe, P., Huth, H., Zhang, J., & Zhao, X. 2011, M&PSA, 46, A138
Lodders, K. 2003, ApJ, 591, 1220
Lodders, K., & Fegley, B. 1999, in IAU Symp. 191, Asymptotic Giant Branch Stars, ed. T. Le Bertre, A. Lebre, & C. Waelkens (San Francisco, CA: ASP), 279
Messenger, S., Keller, L. P., & Lauretta, D. S. 2005, Sci, 309, 737
Messenger, S., Keller, L. P., Stadermann, F. J., Walker, R. M., & Zinner, E. 2003, Sci, 300, 105
Miao, B., Lin, Y., & Wang, D. 2007, M&PSA, 42, A106
Mikouchi, T., Koizumi, E., Monkawa, A., Ueda, Y., & Miyamoto, M. 2003, in 34th Lunar Planet. Sci. Conf., ed. S. J. Mackwell (League City, TX: LPI), abstract 1883
Min, M., Waters, L. B. F. M., de Koter, A., et al. 2007, A&A, 462, 667
Molster, F. J., Waters, L. B. F. M., Tielens, A. G. G. M., Koike, C., & Chihara, H. 2002, A&A, 382, 241
Nagashima, K., Krot, A. N., & Yurimoto, H. 2004, Natur, 428, 921
Nagahara, H., & Ozawa, K. 2009, in 40th Lunar Planet. Sci. Conf., ed. S. J. Mackwell (Woodslands, TX: LPI), abstract 2158
Nguyen, A. N., Nittler, L. R., Stadermann, F. J., Stroud, R. M., & Alexander, C. M. O'D. 2010, ApJ, 719, 166
Nguyen, A. N., Stadermann, F. J., Zinner, E., et al. 2007, ApJ, 656, 1223
Nguyen, A. N., & Zinner, E. 2004, Sci, 303, 1496
Nittler, L. R., Alexander, C. M. O'D., Gao, X., Walker, R. M., & Zinner, E. 1997, ApJ, 483, 475
Nittler, L. R. 2007, Chrono. Meteorit. Early Solar Sys., 125
Nittler, L. R., Alexander, C. M. O'D., Gallino, R., et al. 2008, ApJ, 682, 1450
Nittler, L. R., & Hoppe, P. 2005, ApJL, 631, L89
Nollett, K. M., Busso, M., & Wasserburg, G. J. 2003, ApJ, 582, 1036
Nuth, J. A., Hallenbeck, S. L., & Rietmeijer, F. J. M. 2000, JGR, 105, 10387
Rauscher, T., Heger, A., Hoffman, R. D., & Woosley, S. E. 2002, ApJ, 576, 323
Rietmeijer, F. J. M., Nuth, J. A., III, & Karner, J. M. 1999, ApJ, 527, 395
Stadermann, F. J., Croat, T. K., Bernatowicz, T. J., et al. 2005, GeCoA, 69, 177
Stadermann, F. J., Floss, C., Bose, M., & Lea, A. S. 2009, M&PS, 44, 1033
Stadermann, F. J., Floss, C., & Wopenka, B. 2006, GeCoA, 70, 6168

Stroud, R. M., Floss, C., & Stadermann, F. J. 2009, in 40th Lunar Planet. Sci. Conf., ed. S. J. Mackwell (Woodslands, TX: LPI), abstract 1063
Tielens, A. G. G. M. 2005, The Physics and Chemistry of the Interstellar Medium (Cambridge: Cambridge Univ. Press)
Timmes, F. X., Woosley, S. E., & Weaver, T. A. 1995, ApJS, 98, 617
Vanhala, H. A. T., & Boss, A. P. 2000, ApJ, 38, 911
Vollmer, C., Brenker, F. E., Hoppe, P., & Stroud, R. M. 2009a, ApJ, 700, 774
Vollmer, C., Hoppe, P., Brenker, F. E., & Holzapfel, C. 2007, ApJL, 666, L49
Vollmer, C., Hoppe, P., Stadermann, F. J., et al. 2009b, GeCoA, 73, 7127
Wasserburg, G. J., Boothroyd, A. I., & Sackmann, I. J. 1995, ApJL, 447, L37
Waters, L. B. F. M., Molster, F. J., de Jong, T., et al. 1996, A&A, 315, L361
Woosley, S. E., & Weaver, T. A. 1995, ApJS, 101, 181
Xu, Y. C., Amari, S., Gyngard, F., Zinner, E., & Lin, Y. 2012, M&PSA, 47, 5104
Yada, T., Floss, C., Stadermann, F. J., et al. 2008, M&PS, 43, 1287
Zhao, X., Floss, C., Stadermann, F. J., Bose, M., & Lin, Y. 2011a, in 40th Lunar Planet. Sci. Conf., ed. S. J. Mackwell (Woodslands, TX: LPI), abstract 1982
Zhao, X., Floss, C., Stadermann, F. J., Lin, Y., & Bose, M. 2011b, M&PSA, 46, A261
Zinner, E. 2007, in Treatise on Geochemistry, Vol. 1, ed. H. D. Holland & K. K. Turekian (Oxford: Elsevier), 1